Universidade do Minho
Escola de Ciências

Dora Nazaré Marques

Myopia and Colour Vision, a Case Study

outubro de 2016

Dora Nazaré Marques **Myopia and Colour Vision, a Case Study**

UMinho | 2016

Universidade do Minho
Escola de Ciências

Dora Nazaré Marques

Myopia and Colour Vision, a Case Study

Dissertação de Mestrado
Mestrado em Optometria Avançada

Trabalho realizado sob orientação do
Professor Doutor Jorge Manuel Martins Jorge
e do
Professor Doutor João Manuel Maciel Linhares

outubro de 2016

ACKNOWLEDGMENTS

I would like to express my outmost gratitude to my advisors, Professor Jorge Manuel Martins Jorge and Professor João Manuel Maciel Linhares, for all their support, guidance, knowledge, and patience.

I would like to thank my parents, family and friends for their love, friendship and support.

I would also like to thank my friends of the CEORlab and the Colour Science Lab for all their help.

And I would like to thank the participants, both ametropic and emmetropic, for their kindness and availability, and all those who somehow contributed to the completion of this work.

ABSTRACT

The increasing prevalence of myopia has become a major cause for concern since high myopes are at risk of developing pathologic myopia and blindness. Several structural and functional differences have been identified between a myopic and a normal eye. The myopic eye is usually more elongated and stretched than the normal eye. The excessive elongation of the eye causes a lower packing density of the photoreceptors in the retina, and the electric activity of the retinal neurons is diminished in high myopes. Therefore, it is possible that the chromatic discrimination in myopes is worse than in normal subjects.

The aim of this thesis was to assess the differences in the chromatic discrimination thresholds between non-myopic and myopic subjects.

Forty-two healthy young adults were enrolled in this case study. First, habitual prescription and axial length were measured and ocular health was assessed, including visual acuity, retinography, biomicroscopy, tonometry and wavefront aberrometry. Afterwards, the chromatic discrimination thresholds were determined from the Colour Assessment and Diagnosis (CAD) test and the Cambridge Colour Test (CCT) data. Participants were divided in four groups in accordance to their refractive error (non-, low, moderate and high myopes), and in three groups of axial length (small, medium and long eyes).

It was found that the CAD test has more sensitivity in detecting discrimination differences between the groups, and that the CCT is unable to detect such differences. High myopes have significantly increased chromatic discrimination thresholds in the CAD test, in general, and in the red and blue regions of the colour space than the other groups. The results suggest that the chromatic discrimination in high myopes is significantly worse than non- and low-to-moderate myopes and that the CAD test may be useful in determining such differences.

RESUMO

A elevada prevalência de alta miopia a nível mundial tem sido encarada como um problema de saúde pública. O comprimento axial excessivo característico da alta miopia pode acarretar complicações oculares patológicas e eventualmente resultar em cegueira. A densidade dos fotorreceptores na retina dos míopes difere da dos não-míopes, sendo menor nos primeiros dado o maior comprimento axial do olho míope, e a resposta neuronal obtida a partir de electroretinografia é diminuída nos altos míopes. Assim, pode acontecer que a perceção cromática seja diferente entre míopes e não-míopes e, para tal, os limiares de deteção cromática de ambos foram determinados.

O objetivo deste trabalho é o de determinar a discriminação cromática de sujeitos míopes e não míopes e avaliar a sua diferença.

Este caso de estudo incluiu 42 jovens adultos saudáveis. Primeiro, determinou-se a correção habitual e o comprimento axial, bem como a acuidade visual. A saúde ocular foi avaliada recorrendo a biomicroscopia, retinografia, tonometria e aberração de frente de onda. De seguida, os limiares de deteção cromática foram determinados dos dados obtidos pelo teste Colour Assessment and Diagnosis (CAD) e o Cambridge Colour Test (CCT). Os participantes foram divididos em 4 grupos refrativos (não-míopes, baixos-, moderados- e altos-míopes), e 3 grupos de comprimento axial (olhos pequenos, médios e grandes).

Comparando ambos os testes, o CAD parece ser mais sensível na determinação de alterações da perceção cromática, pois apresenta uma correlação estatisticamente significativa com o comprimento axial e o erro refrativo, ao contrário do CCT. Detetou-se um aumento estatisticamente significativo dos limiares de deteção cromática determinados com o CAD dos altos-míopes em comparação com os restantes grupos, em particular nas regiões vermelha e azul. Os resultados apontam para uma pior perceção cromática dos altos míopes do que a dos não-míopes e baixos/moderados-míopes e o CAD aparenta ser um teste útil na deteção destas diferenças.

INDEX

Abbreviations and Acronyms

AOSLO: Adaptive Optics Scanning Laser Ophthalmoscopy

B: Blue

C': Negative cylinder

CAD: Colour Assessment and Diagnosis

CCT: Cambridge Colour Test

CH: Corneal hysteresis

CIE: Commission Internationale de l'Eclairage

CRF: Corneal resistance factor

EM: Electromagnetic

ETDRS: Early Treatment of Diabetic Retinopathy Study

ffERG: Full-field electroretinography

G: Green

GCL: Ganglion cell layer

H: Horizontal cells

HOA: Higher order aberrations

ILM: Internal limiting membrane

INL: Inner nuclear layer

IOP: Intraocular pressure

IOPcc: Corneal compensated intraocular pressure

IOPg: Goldmann correlated intraocular pressure

IPL: Inner plexiform layer

J_0: Vertical astigmatism component

J_{45}: Oblique astigmatism component

LGN: Lateral geniculate nucleus

LogMAR: Units of measurement of visual acuity by the logarithm of the Minimum Angle of Resolution

M: Mean spherical equivalent component

mERG: Multifocal electroretinography

NFL: Nerve fibre layer

OLM: Outer limiting membrane

ONL: Outer nuclear layer

OPL: Outer plexiform layer

Q1: Red quadrant of the Cambridge Colour Test

Q2: Yellow quadrant of the Cambridge Colour Test

Q3: Green quadrant of the Cambridge Colour Test

Q4: Blue quadrant of the Cambridge Colour Test

R: Red

RMS: Root mean square

RPE: Retinal pigment epithelium

S: Mean sphere

V1: Striate visual cortex or visual area 1

Y: Yellow

α: Cylindrical axis

INDEX OF FIGURES

INDEX OF TABLES

1. Literature Review

1.1. The Visual System

The human eye can be divided into three main layers: the sclera, the uvea and the retina. These layers surround three transparent structures that are responsible for the refraction and transmission of light, from the outside of the eye into its inside, which are the aqueous humour, the vitreous humour and the crystalline lens[1,2] (Figure 1).

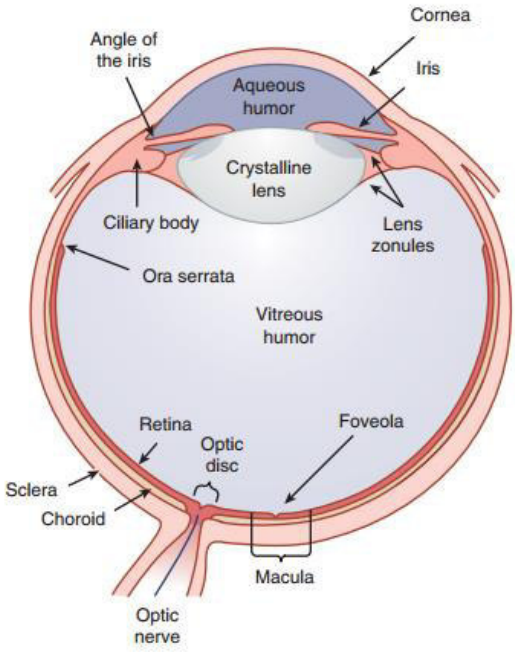

Figure 1. Cross section of the three main layers of the human eye. Adapted from Schwartz 2010.

The outer layer of the eye contains the cornea and the sclera[1]. The cornea is a transparent tissue that protects the eye and acts as a refractive lens. It is responsible for most of the refractive power of the eye (two-thirds), with about 43 D[3]. The sclera is a white connective tissue coat responsible for the support and protection of the eye and is connected to the cornea through the limbus[1,2].

The middle layer, or the uvea, contains the iris, the ciliary body and the choroid[4]. The iris is responsible for pupil size and for the amount of light that enters the eye. It constricts in response to higher light levels and dilates when the light level drops[1,2].

The choroid is a pigmented vascular tissue and is mainly responsible for the blood and nutrient supply to the retina[2].

The ciliary body is responsible for the accommodation of the crystalline lens and the production of aqueous humour. The ciliary muscle of the ciliary body is able to alter the shape of the lens and its power, making it possible for the eye to focus on near or far stimuli, fluidly – a process called accommodation. The lens is responsible for about one-third of the refractive power of the eye, and has a dioptric power of 20 D[3], so a transparent lens is of great importance. Any change to the lens transparency will prevent the light to seamlessly progress into the retina.

The aqueous humour is responsible for the nutrition and the support of the internal structures of the eye, such as the cornea and the lens. The eye drains the aqueous humour through the channel of Schlemm. It maintains an intraocular pressure (IOP) of about 16 mm Hg that is responsible for the structural integrity of the eye. In case of an elevated IOP, when there is an overproduction and/or poor drainage of the aqueous, ganglion cells start to die and retinal damage occurs[1], with great impact on the eye peripheral vision first and central vision later.

The vitreous humour is in the posterior chamber, and it fills the space from the lens and ciliary structures to the retina. It is mostly made of collagen and hyaluronic acid and is responsible for the structural support of the retina[2]. Finally, the inner layer, the retina, acts as the sensory layer of the eye[4].

1.1.1. Retina

The human retina is a complex nervous tissue responsible for capturing and processing the light that enters the eye[5] (Figure 2). It has six major types of distinct cells in its layers. Light first passes through the retinal inner layers and then on to the photoreceptors in the outer layers[5].

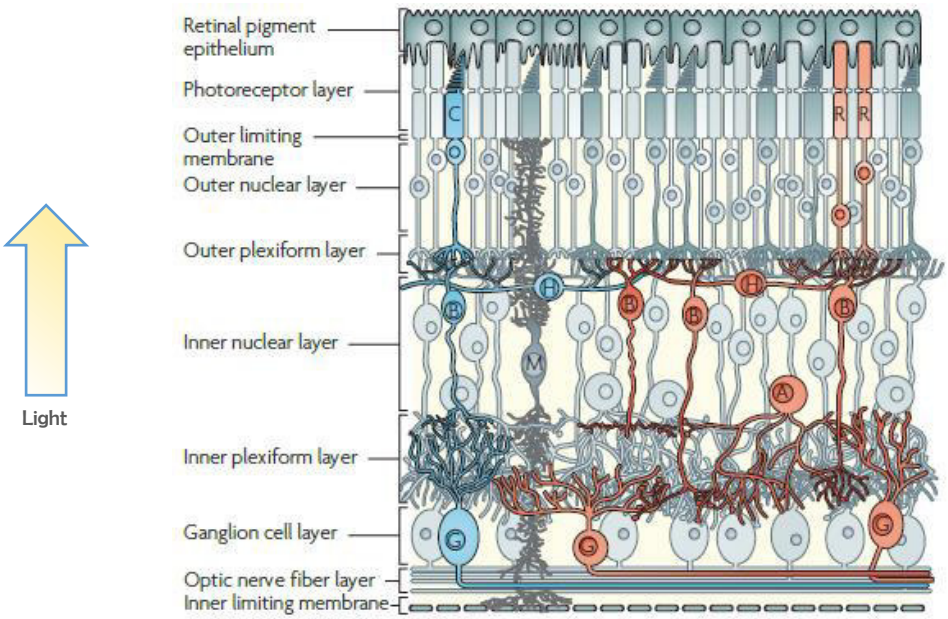

Figure 2. Cross section of the human retinal layers and their major cell types: cones (C) and rods (R); bipolar cells (B); horizontal cells (H); amacrine cells (A); Müller glial cells (M) and ganglion cells (G). Light passes through the inner limiting membrane and the inner retina before reaching the photoreceptors. Adapted from Swaroop, Kim & Forest 2010.

The retinal pigment epithelium (RPE) is the outer layer of the retina. It is mainly responsible for the nutrition of the photoreceptors[1,6], for the phagocytosis of the products they release[7] and for the diminishing of light scattering[8] by absorption by its dark pigment, which contributes for a clear image in the normal eye.

Photoreceptors are near the choroid for blood supply and the maintenance of their metabolic activity. They make the outer limiting membrane (OLM) and the outer nuclear layer (ONL). Next to them are the outer plexiform layer (OPL), which connects the photoreceptors to the bipolar and horizontal cells, and the inner nuclear layer (INL), which contains their cell bodies, as well as Müller glial and amacrine cells[5,6]. Both rods and cones are connected to bipolar cells. Horizontal cells connect the bipolar cells to the photoreceptors horizontally. Amacrine cells connect the bipolar cells to the ganglion cells also horizontally. Müller glial cells are responsible for trophic and neuroprotection functions and interact with most of the other retinal cells[9,10].

The inner plexiform layer (IPL) is comprised by the axons of the bipolar and amacrine cells, which connect to the ganglion cells in the ganglion cell layer (GCL). Next to this layer is the nerve fibre layer (NFL), which contains the axons of the ganglion cells. These form the optic nerve that synapses in the brain[1,6]. The previous layers are limited by the internal limiting membrane (ILM), between the retina and the vitreous humour[1].

1.1.2. Photoreceptors

There are two types of photoreceptors: rods, responsible for scotopic vision or low light level vision, and cones, responsible for photopic vision or higher light level vision[1,6]. Rods and cones, together, are responsible for mesopic vision (twilight)[1]. Photoreceptors can be divided in an inner and an outer segment. The inner segment consists of the cell body and the synaptic pedicle. The outer segment contains visual pigment molecules in a stack of disks, with two main components: opsin and retinal (Figure 3). Opsin is a large protein that determines the absorption characteristics of the molecule[11]. The cones mediate colour vision and there are three distinct types of cones in the human retina: short- (S-), middle- (M-), and long- (L-), wavelength-sensitive-cones. Each class of cone has a different opsin. In contrast, there is only one type of rod opsin[12]. Retinal is a light-sensitive molecule that is identical for all cone photopigments. When the retinal absorbs one photon of light, a series of events take place that result in the transformation of light into electrical signals. This process is called visual transduction[8,11].

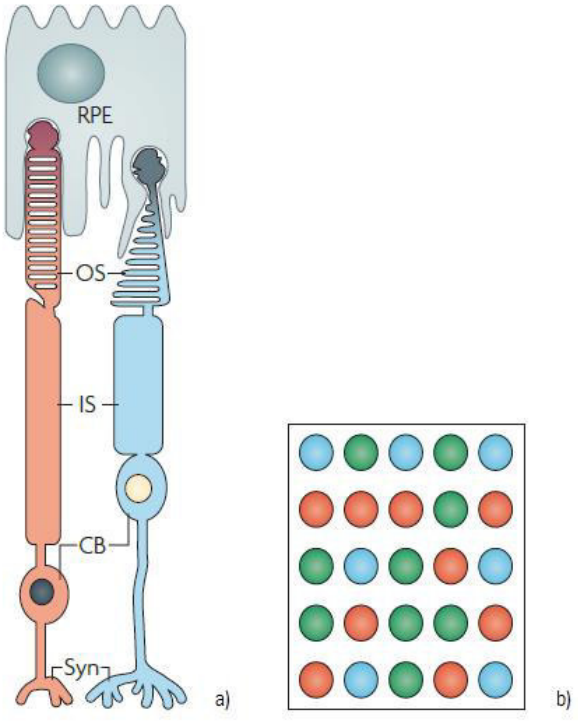

Figure 3. a) Cone and rod photoreceptors: outer segment (OS) (connected to the retinal pigment epithelium (RPE)), inner segment (IS), cell body (CB) and synaptic pedicle (Syn). b) Human cone photoreceptor distribution mosaic: Short-, medium- and long-wavelength sensitive cones, represented in blue, green and red, are randomly distributed in the retina. Adapted from Swaroop, Kim & Forest 2010.

Photoreceptors are differently distributed across the retina. The fovea, an avascular area of the central retina, contains only cones, in a total of about 1 percent (50 000) of the cones in the retina. At the centre of the fovea, there is a region comprised only by M- and L-cones and without S-cones, the foveola[13]. The peripheral retina contains both cones and rods, in a total of about 6 million cones and 120 million rods. In the blind spot, the area where the optic nerve leaves the eye, there are neither cones nor rods[11].

The cone distribution in the retina seems to be random, both in the centre as well as in the periphery[14]. A study involving Adaptive Optics Scanning Laser Ophthalmoscopy (AOSLO) imaging has shown that more than 90% of the human cone mosaic consisted of L- and M-cones and only 5-10% S-cones[15]. Although with high variation, L-cones tended to outnumber the M-cones[15], which is consistent with other studies[15,16]. Nevertheless, this variation does not seem to affect colour vision[17]. As far as for S-cones, they also seem to have a random distribution in the human retina[18].

A study on the photoreceptors packing density has shown a high variability in the distribution both between and within individuals. Curcio and collaborators[19] found a distribution range of 100,000 to 324,000 cones/mm^2 in eight cadaver retinas and a mean cone estimation of about 199,000 cones/mm^2. Cone density was higher in the horizontal meridian, especially in the nasal quadrant (40 to 45% higher) and decreased with increasing eccentricity in the temporal, inferior and superior quadrants, respectively. Rod density was also higher in the nasal quadrant, followed by the temporal, superior and inferior quadrants. The rod-free zone in the fovea had a horizontal oriented ellipse shape with a ratio of 1.29, where the horizontal diameter was 0.350 mm, or 1.25°. In turn, rod density ranged between 77.9 to 107.3 million in the retina, with higher density in the superior quadrant. Other studies have found similar results[20–22].

Retinal neurons use pooling to transmit information. There are nearly 130 million photoreceptors in the human retina, but only 5 million bipolar cells and 1 million ganglion cells[5]. Therefore, the electrical signals must be pooled together throughout the retina[11]. Since there are many more rods than cones, rod signals are much more pooled than cone signals, in an average of 120 rods to one ganglion cell against an average of 6 cones to one ganglion cell, while in the foveola there is up to a 1 to 1 connection. As a result, rods have greater sensitivity and respond faster than cones, but cones have better visual acuity and detailed vision[11].

1.1.3. Post-retinal Pathways

Once the optic nerve leaves the retina, it projects the information onto the optic chiasm, where the ganglion cell fibres from the nasal retina cross over to join the temporal fibres of the contralateral eye. The right optic tract will carry the information from the left visual field and vice versa[1,23] (Figure 4).

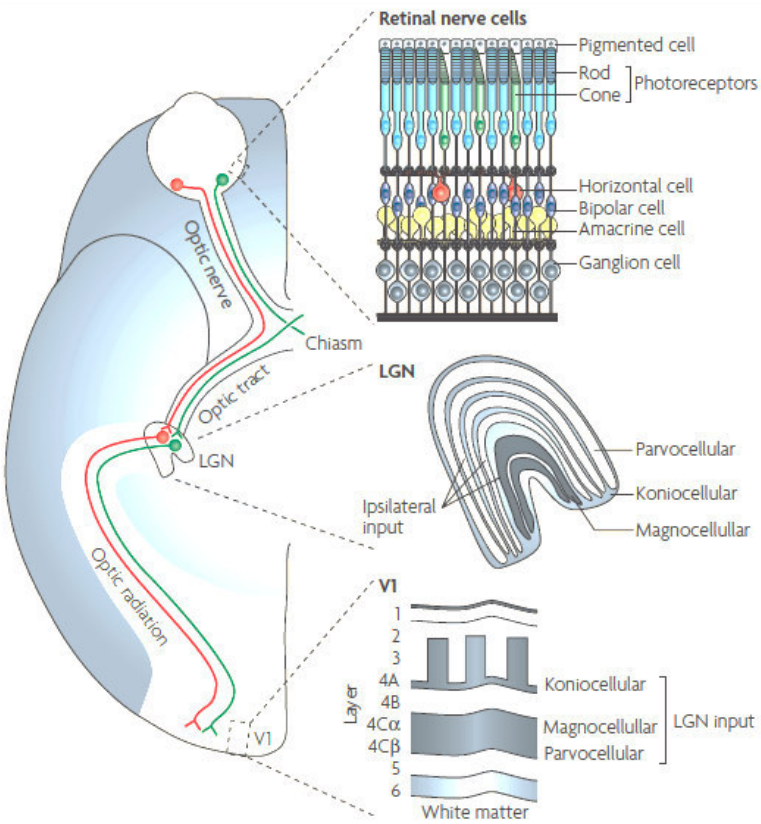

Figure 4. Visual pathway. Information from the retinal nerve cells passes through the optic nerve, and the information from the nasal retinas is crossed in the optic chiasm. The optic tract conducts the information to the lateral geniculate nucleus (LGN) layers. Cortical area V1 receives the information from the three pathways of the LGN. Adapted from Solomon & Lennie 2007.

The optic tract transmits information to the lateral geniculate nucleus (LGN), which has six layers. Layers 1, 4 and 6 receive input from the contralateral eye and layers 2, 3 and 5 receive input from the homolateral eye. The LGN has three parallel pathways that process different features of the retinal image: the parvo, the magno and the konio retinogeniculate pathways. The four lateral layers of the LGN consist of parvo cells and the two medial layers consist of magno cells. These layers are intercalated by the konio cells. The parvo pathway is involved in detailed and red-green colour vision. The magno pathway encodes luminance and fast movement. The konio pathway is involved in yellow-blue colour vision[1].

The axons of the LGN end in the striate visual cortex or visual area 1 (V1), the cortical area of the cerebral cortex: parvo cells project to layer 4Cβ, magno cells to layer 4Cα, and konio cells to lower layer 3 and layer 4A[23]. The cells of the striate visual cortex project their axons to nearby cortical areas of vision in the extra-striate visual cortex, and from there onto several higher cortical areas. These will be partly responsible for the integration of visual information with memory and other sensory perceptions[1].

1.2. Colour Vision

1.2.1. Light and Colour

Visible light is the part of the electromagnetic (EM) spectrum that is detected by the human eye (Figure 5). It ranges from 400 (short-wavelengths) to 780 nm (long-wavelengths). Wavelengths from about 400 to 450 nm are perceived as violet; 450 to 490 nm, as blue; 500 to 575 nm, as green; 575 to 590 nm, as yellow; 590 to 620 nm, as orange; and 620 to 780 nm, as red[11], by colour normal observers.

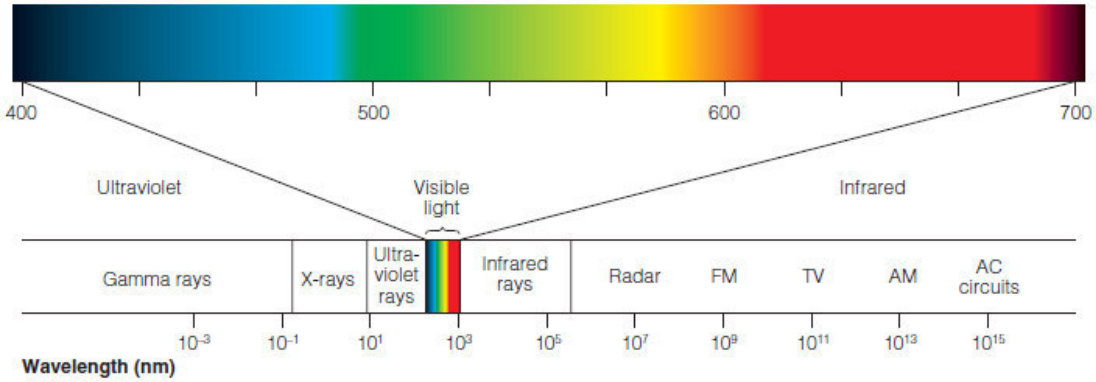

Figure 5. The electromagnetic spectrum. Visible light is only a small part of the spectrum. Wavelength is in nanometres (1 nm=10^{-9} m). Adapted from Goldstein 2013.

The amount of the wavelengths of the light spectrum reflected by an object is responsible for the colour perception, and produces the hue of the object, like red, green or blue[11]. The probability of a cone absorbing a photon of a given wavelength depends on the wavelengths that reach the eye, in terms of the number of photons per wavelength (principle of univariance)[24]. This determines the spectral sensitivity of a cone, which is different for each cone class. The genes of the three cone types, S, M and L, that are responsible for the three maximum photon absorptions

have been isolated and sequenced, and their opsins have been identified in the past[25]. Their maximums lie in the short- (419 nm), middle- (531 nm) and long-wavelength (558 nm) sections of the visual spectrum[12,26,27]. The overlap between the L- and M-cone absorption spectra allows for the combination of the cone signals and improves visual acuity at the fovea[28]. Thus, colour vision at the photoreceptors level is trichromatic and is mediated by these three cone types[29]. Rods have their absorption peak in 500 nm[12], but are not involved in colour vision[2].

Changes to the spectral sensitivity of the cones of the eye may have an impact on the colour perception of the colours that reach the eye. If the three cone types are present but their maximum sensitivity is shifted, these observers are called anomalous colour vision observers, specifically deuteranomalous (a shift on the M-cone) or protanomalous (a shift on the L-cone). A great variability of shifts is commonly found on the S-cone of normal colour vision observers, and as such there is no classification of a tritanomaly observer. If one of the cone types is missing, the observer is called dichromat: protanope, deuteranope and tritanope if the L-, M- or S- cone is missing, respectively. Other types of colour vision deficiency are possible (for example monochromacy), but will not be further explored in this work[29].

Regarding the ganglion cell information processing, colour perception is converted into opponent processes due to three neural mechanisms: two opponent channels for colour and a luminance channel. In the luminance or L+M channel, L- and M-cones signals are summed to compute the intensity of a stimulus. In the red-green or L–M colour opponent channel, the signals of L- and M-cones are subtracted from each other to compute the red-green component of a stimulus. In the yellow-blue or S–(L+M) opponent channel, the sum of the signals of L- and M-cones is subtracted from the signal of S-cones to compute the yellow-blue component of the stimulus. These channels match the three pathways of the LGN described before[30,31].

1.2.2. Chromaticity Diagrams: The CIE Colour Specification System

In 1931, the Commission Internationale de l'Eclairage (CIE) created the CIE colour space chromaticity diagram, commonly referred to as the *x, y chromaticity diagram*. It works as an objective colour measurement system to match the colour perception of a given observer. The colours in the diagram are specified based on the trichromatic colour matching results of a normal trichromatic observer with a 2° field of view[29].

In the CIE 1931- *x, y* chromaticity diagram, all colours can be matched with the mixture of positive amounts of three primaries in the red, green and blue regions of the electromagnetic spectrum, by varying the amount of each primary in the match[29,32]. Consequently, the adding of the three primaries in equal amounts will produce white. However, sometimes the trichromatic mixture is too desaturated to match the test colour exactly, so, in order to obtain the exact match, an additional desaturating colour must be added to the test colour[29]. To do so, it requires the use of imaginary colours, or primaries[29]. The CIE primaries are designated as X, Y and Z, and their relative amounts are *x*, *y* and *z* [33]:

$$x = \frac{X}{X + Y + Z}$$

$$y = \frac{Y}{X + Y + Z}$$

$$z = \frac{Z}{X + Y + Z}.$$

The sum of these amounts equals 1, so only two amounts, *x* and *y*, need to be quantified, and the total colour range can be represented in a two-dimensional diagram for each luminance level[29]. This means that white and all grey shades are mapped in the same coordinate. Also, many browns are mapped in the same coordinates as yellows and oranges. All additive mixtures of pairs of colours must lie along a straight line that connects them, hence the shape of the diagram[32]. For instance, the bottom line from the short- to the long-wavelength is known as the purple boundary as it includes all the purple colours that come from the mixture of violet and red[33] (Figure 6).

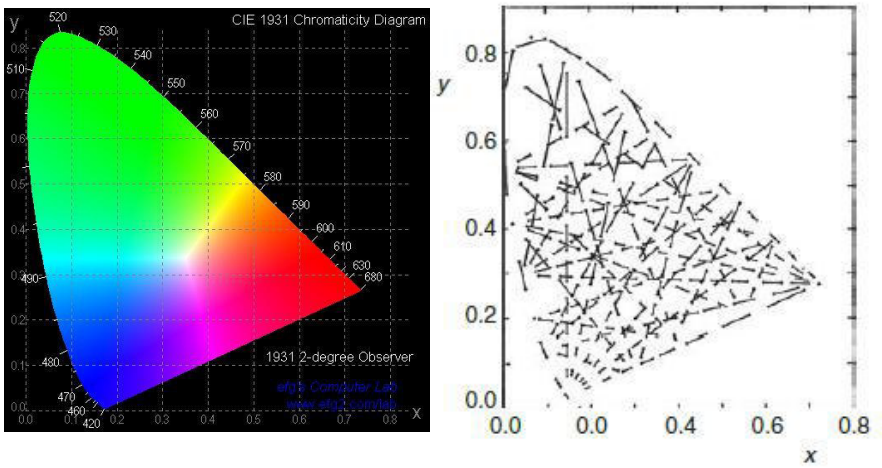

Figure 6. The CIE-*x, y* 1931 chromaticity diagram. On the left, x and y are the coordinates that represent chromaticity coordinates. All the monocromatic colours experiences lie along the limiting contour, ranging from 380 to 780 nm. All the other colours result form combinations of these colours. On the right, each line represents a perceptual colour difference of the same magnitude and luminance across the diagram. The length of the lines should be the same for uniformity purposes. Adapted from http://www.efg2.com (left) and Hunt & Pointer 2011 (right).

The CIE-*x*, *y* 1931 chromaticity diagram has the disadvantage of a highly non-uniform colour distribution. When plotting two colours of a perceptual difference of the same magnitude and luminance, their representation in the diagram is very different – the lines have very different lengths[33], as is represented on the right hand side of Figure 6. In order to minimize this effect, CIE created a new diagram with the same properties as the previous one and based on it, but with different chromaticity coordinates – the CIE 1976 uniform chromaticity scale (UCS) diagram, commonly referred to as the *u', v' diagram* –, which is obtained by plotting *u'* against *v'* (Figure 7). On the right hand side of Figure 7, the uniformity can be ascertained by observing the higher regularity in the length of the plotted lines, and where[33]:

$$u' = \frac{4X}{X + 15Y + 3Z} = \frac{4x}{-2x + 12y + 3}$$

$$v' = \frac{9Y}{X + 15Y + 3Z} = \frac{9y}{-2x + 12y + 3}$$

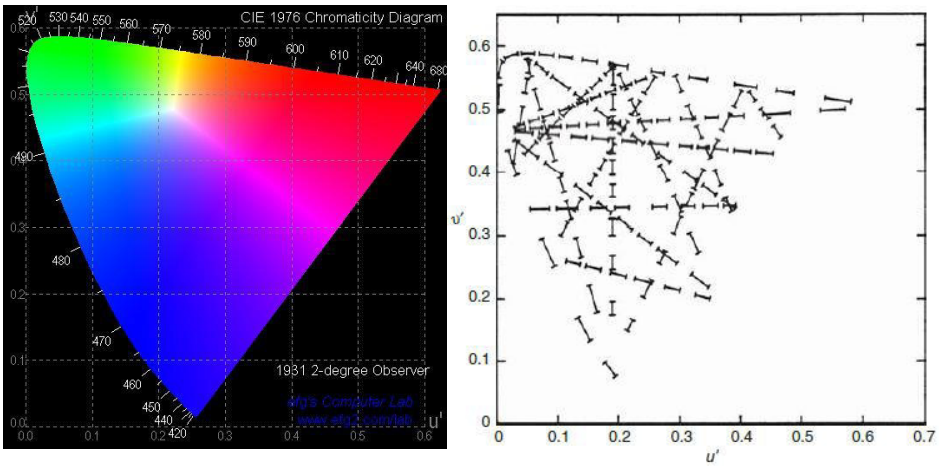

Figure 7. The CIE 1976- *u', v'* uniform chromaticity diagram, with *u', v'* coordinates. On the left, additive mixture of colours are represented by points lying on the straight line joining the points that represent constituent colours, ranging from 380 to 780 nm. On the right, each line represents a perceptual colour difference of the same magnitude and luminance. The lengths of the lines are more similar than for the *x, y* coordinates. Adapted from http://www.efg2.com (left) and Hunt & Pointer 2011 (right).

The *u', v'* diagram is very useful for tracing the confusion lines which consist of the positions of colours of equal luminance likely to be confused by observers that do not have a normal colour vision perception, but the *x, y* is still the norm[33].

In chromaticity diagrams, the chromatic discrimination of an observer is represented by a series of ellipses. The size of each ellipse varies according to the chromaticity coordinates of the

colour under testing and represents the ability of the observer to distinguish colours[29]. The larger the ellipse, the poorer the chromatic discrimination of the observer.

1.2.3. Colour Confusion Lines

Colour confusion lines include all colours that are indistinguishable for dichromats, who lack one of the cone types. All the sets of confusion lines originate from the same virtual point for each defect (Figure 8). Confusion lines are why protan (L-cones missing) and deutan (M-cones missing) defects are often referred to as red-green, because a protan confuses blue-green with red and a deutan confuses blue-green with reddish purple. On the other hand, a tritan defect is also referred to as blue-yellow because they confuse blue-violet and yellow stimuli[1].

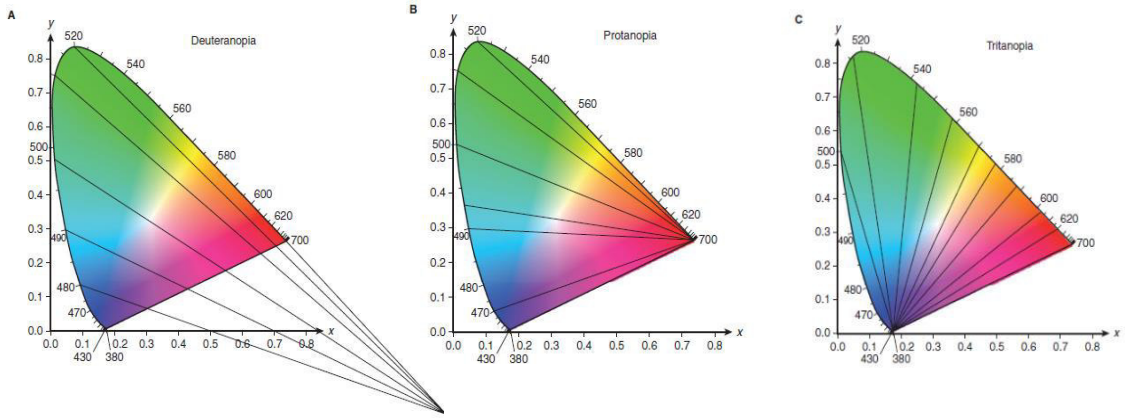

Figure 8. Colour confusion lines plotted on the CIE-*x, y* 1931 chromaticity diagram for (A) deutan, (B) protan and (C) tritan subjects. All lines origin at a different point for each colour vision defect. Adapted from Schwartz 2010.

1.2.4. Colour Vision Tests

There are several colour vision tests that are used in clinical practice to identify and grade colour vision deficiencies[29]: screening tests (normal or abnormal colour vision); classifying tests (in protan, deutan or tritan defect); grading tests (for the severity of the defect); diagnosis tests (type of deficiency, dichromat or anomalous trichromat), and, finally, occupational tests (selection of personnel for specific occupations that require good colour vision). They can also be used to assess some retinal pathologies and their effects on colour vision and to measure their progression[34].

The psychophysical methods used for colour vision tests are varied. Visual tasks may consist of colour matching, identification of a figure, arrangement of a sequence of hues or colour

naming. Currently, the widest application tests for colour vision screening are pseudoisochromatic tests[29].

Pseudoisochromatic tests involve the identification of a figure. Test plates are made of coloured patches that vary in size and lightness and that are placed in a way that a normal colour vision observer is able to correctly identify the figure, but a colour deficient observer is not. That is due to the fact that the figure and the background are coloured within isochromatic regions based on colour confusion lines that seem to have the same colour to them. Also, the circular patches in a matrix design helps disguising the outline and the shape of the figure[29].

Computerized pseudoisochromatic tests usually use a staircase procedure to grade the defect severity[29]: the test starts with an easily detectable stimulus over its background that decreases intensity (in saturation) each time the subject responds correctly, until an error occurs. This is a crossover point, when the stimulus is not differentiated from its background. The next stimuli presented are made easier to detect until the participant is able to detect them again over the background. This is another crossover point. At this point the threshold is the mean value between the two crossover points. This procedure is then repeated several times and, in the end, the chromatic thresholds of the observer are obtained by averaging the crossover points[11].

Only two computerized colour vision tests will be used in this work and hence described fully: the Cambridge Colour Test (CCT) and the Colour Assessment and Diagnosis Test (CAD).

1.2.4.1. Cambridge Colour Test

The Cambridge Colour Test (CCT) allows the screening of colour vision deficiencies and the monitoring of changes in colour discrimination that occur due to congenital or acquired colour vision deficiencies[35].

The CCT is based on the pseudoisochromatic principles described above. It consists of a C shaped target that differs in chromaticity from the background (Figure 9). Both the target and the background consist of discrete colour patches of randomized luminance. Each patch has its own contour. The C is randomly presented in four different positions – up, down, left and right – and the observer must identify the orientation of the gap of the letter. It is presented in several levels of saturation and hue along the confusion lines of the protan, deutan and tritan defects. The

difference in chromaticity between target and background is adjusted according to the performance of the observer[35,36]. The bigger the difference, the worst the chromatic discrimination of the observer.

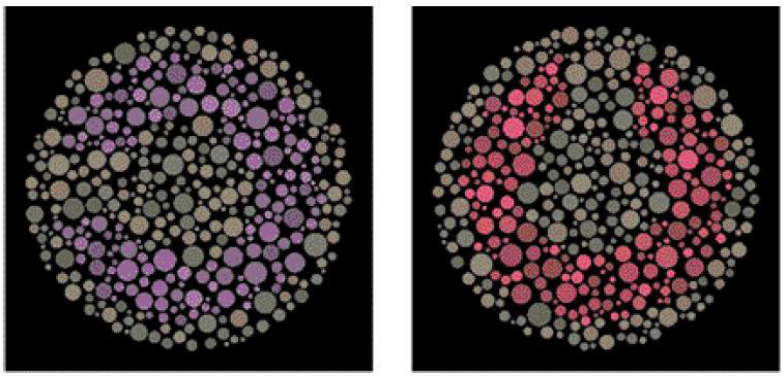

Figure 9. C-shaped target of the Cambridge Colour Test with two different orientations. Adapted from Mollon & Regan 2000.

This test determines the step sizes of the staircases and measures chromatic thresholds within the CIE-*u',v'* 1976 chromaticity diagram, mainly due to its uniformity[35]. The normal result output consists of discrimination ellipses with an axis ratio less than 2.0[35] (Figure 10).

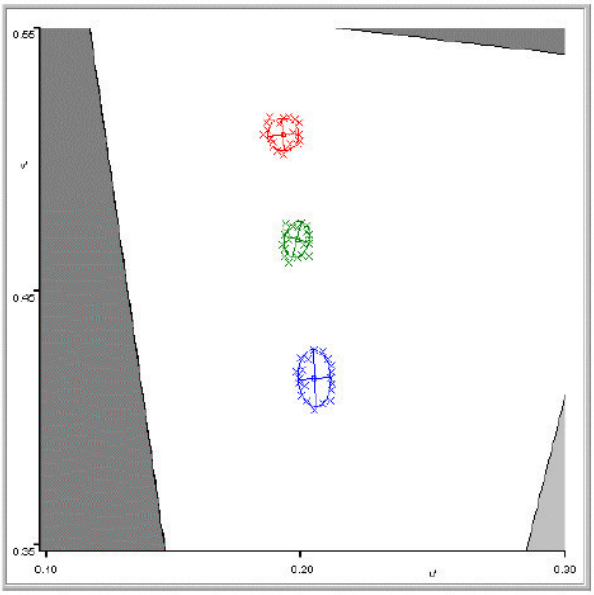

Figure 10. CCT results for a normal observer, with three ellipses from three different background chromaticities. The small crosses are the individual thresholds for the different hue directions. Adapted from Mollon & Regan 2000.

Colour deficient observers will exceed the ratio mentioned above. The direction of the axis of the major ellipse indicates the type of deficiency, and the longer the axis, the more severe the defect is. For protan and deutan defects, the ellipses are horizontal, with a different orientation,

but typically oriented along the confusion lines. For tritan defects, the ellipses are oriented along tritan confusion axes[35] (Figure 11).

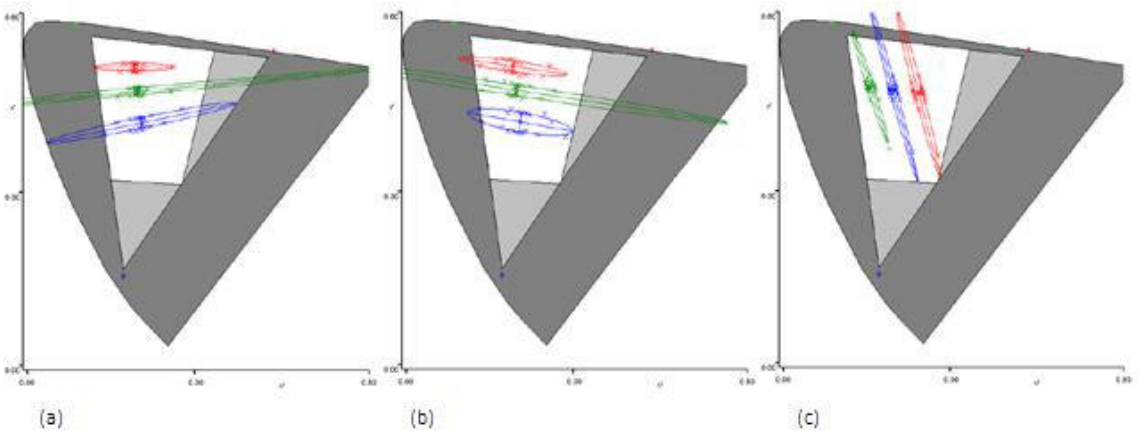

Figure 11. CCT results for colour deficient observers. (a) Protan, (b) deutan and (c) tritan observer. The major axes of the ellipses are oriented along the confusion lines for each deficiency. Adapted from Mollon & Regan 2001.

1.2.4.2. Colour Assessment and Diagnosis Test (CAD)

The CAD test is also based on pseudoisochromatic principles. It presents a diagonally moving coloured square stimulus in a luminance dynamic grey background. It isolates the colour signals in a dynamic luminance contrast noise, so that the observer is unable to use residual luminance signals as clues to detect the test stimulus[37] (Figure 12).

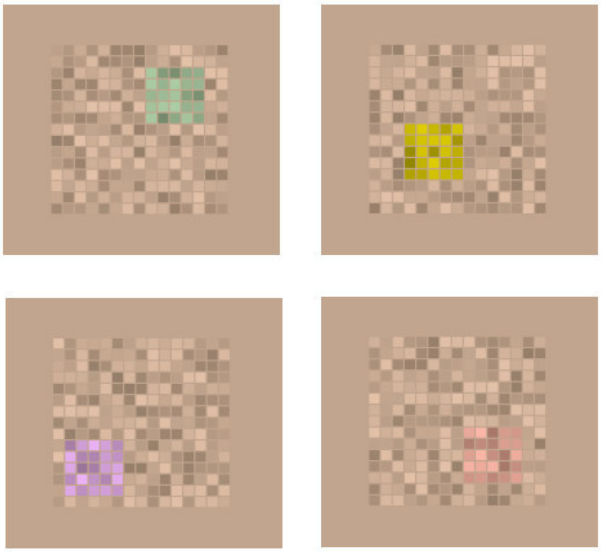

Figure 12. Moving squares in a dynamic background of the CAD test. The coloured square moves randomly in the diagonal and the observer must identify its direction. Adapted from Barbur, Rodríguez-Carmona & Harlow 2006.

The thresholds are measured along several directions of the colour space (different hues), which allows for the measurement of any chromatic sensitivity loss and the classification of minimal defects that are undetected in the standard colour vision tests[38]. The resulting ellipses are plotted on the CIE-*x,y* 1931 chromaticity diagram[38,39].

This test was used to establish the chromatic sensitivity in 250 normal and 300 colour deficient observers[40]. Figure 13 represents the results for a normal trichromat. The grey region represents the normal variability in both red-green and yellow-blue thresholds, including the median (black-dotted ellipse). It is the region in the CIE diagram where the results of 95% of the normal observers lie, and it is limited by the 2.5% and 97.5% corresponding statistical limits. The deutan, protan and tritan confusion bands are displayed in green, red and blue, respectively. The black cross (0.305, 0.323) indicates background chromaticity (*x, y*). The dotted black ellipse represents the median chromatic discrimination threshold for the standard normal observer and allows for the assessment of the severity of colour vision loss[40].

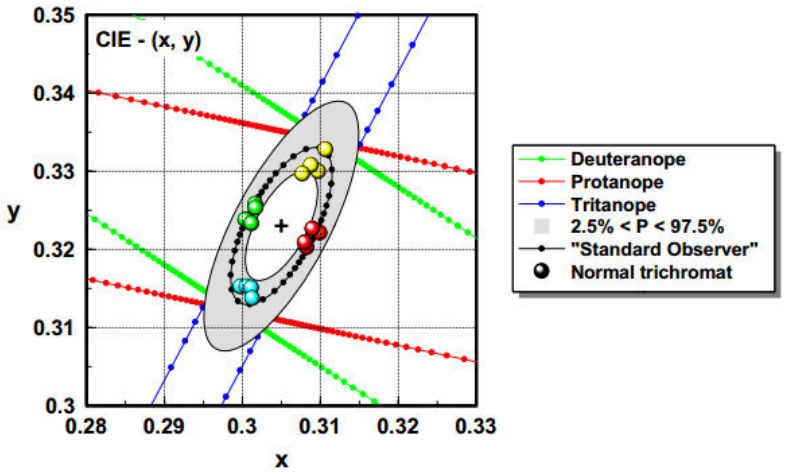

Figure 13. Results of a normal trichromat CAD test observer. The results are plotted in the CIE-*x,y* 1931 diagram. The black-dotted ellipse represents the median for 250 normal trichromats. The grey region represents the threshold limits for 95% of the normal observers. The inner and outermost ellipses are the 2.5% and 97.5% corresponding statistical limits. The deutan, protan and tritan confusion bands are displayed in green, red and blue, respectively. The black cross (0.305, 0.323) indicates background chromaticity (*x,y*). Adapted from Barbur, Rodriguez-Carmona, Evans & Milburn 2009.

The CAD test diagnoses the type of deficiency through the elongation of the ellipses major axis along the deuteranopic (Figure 14, left) or protanopic (Figure 14, right) confusion lines. The higher the chromatic discrimination threshold value, the more severe the defect is[40].

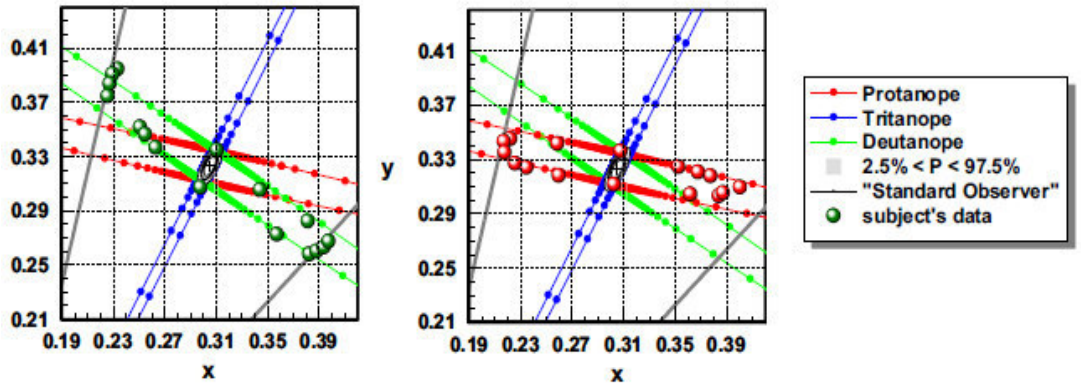

Figure 14. Chromatic thresholds for two colour vision deficient observers with severe colour vision deficiency. Grey lines represent the largest chromatic displacements away from background chromaticity that are set by the isoluminant condition and the limits imposed by the phosphors of the display. The greater the elongation along the deuteranopic (left) or the protanopic (right) confusion lines, the lower the level of chromatic sensitivity and the greater the colour vision loss. Adapted from Barbur et al 2009.

The CCT is the standard computerized test for the fast screening of colour vision deficiencies and acquired defects[34]. On the other hand, the CAD test was developed to detect and measure minimum changes in chromatic sensitivity[39]. It is currently the standard testing protocol for English pilots and traffic controllers[41] and is being applied to underground train drivers[42]. Therefore, different results should be expected in the frontier cases of colour vision anomalies when using both tests.

1.3. Myopia

1.3.1. Myopia and Visual Impairment

Refractive error causes the retinal image of a distant object to be blurred, if uncorrected, and currently is a major cause for visual impairment worldwide[43]. Myopia is the most common refractive error in children from 5-15 years old in the present day[43] and may be corrected with prescription glasses, contact lenses or refractive surgery[44].

Clinically speaking, an eye with an axial length greater than 25 or 26 mm or a refractive error more negative than -6 D is considered highly myopic[45,46]. High myopia is a significant risk factor for visual impairment in the general population and has the highest percentage of bilateral blindness and low vision of all of the refractive errors[47].

1.3.2. Worldwide Prevalence of Myopia

Recent reviews have shown that the prevalence of myopia varies among populations of different ages, regions and ethnicities[48,49]. Children from urban areas and from East Asian countries, namely, China, have the highest myopia prevalence rates[48–50]. Specifically, children from urban areas have 2.6 times higher chances of developing myopia than those from rural ones[50]. As for adults, Asian populations show the highest prevalence of myopia in comparison with Western-based populations, however, this difference is smaller than for children populations[48].

A recent systematic review and meta-analysis studied the global prevalence of myopia and established its temporal trends through the analysis of 145 studies published from 1995 to 2015. This study estimates that in the year 2000 more than 20% of the world population (1406 million people) had myopia, and that by the year 2050 that percentage is expected to increase to nearly 50% (4758 million people). Correspondingly, in 2000, almost 3% of the world population (163 million people) had high myopia, which is expected to increase by 2050 to 10% (938 million people)[51].

1.3.3. Risk Factors for Myopia

Several genes responsible for molecular and biological mechanisms of the eye have been recently identified in the development of refractive error, but environmental factors also seem to have a determinant role, which suggests that myopia is multi-factorial in its origin and depends on both genetic and environmental factors[44,49,52]. The major risk factors that are currently considered to be related to myopia are peripheral refraction, parental myopia, near work activities and time spent outdoors[44,49].

1.3.3.1. Peripheral Refraction

Peripheral refraction is known to be different from the individual refraction. Emmetropes have similar central and peripheral refraction, and a spherical eye shape. Myopic adults usually have a hyperopic peripheral refraction, and hyperopic adults a myopic peripheral refraction[53]. This is also found in children[54,55]. The hyperopic peripheral refraction is associated with an prolate-shaped eye with increased elongation when compared to normal eye, both in myopic children[55] and adults[56].

Animal studies suggest that hyperopic peripheral defocus induces eye growth and, consequently, influences the emmetropization process[57]. Correspondingly, a study involving peripheral refraction in children has shown a change from relative peripheral myopia to relative peripheral hyperopia in those who developed myopia, although the baseline relative to the peripheral refraction did not predict the development or progression of myopia[58].

In other studies, there seems to be an association between peripheral refraction and myopia progression. Peripheral refraction was found to be significantly more hyperopic and the nasal retina was found to be significantly steeper in progressive than in stable young adult myopes[59]. In a different study, the rate of myopia progression was weakly correlated with changes in the peripheral refraction of the nasal retina of four treatment groups of 14 to 22-years-old myopes (altered spherical aberration and vision training, altered spherical aberration only, vision training only, and control), but no significant differences were found between groups[60]. So, a causative link between peripheral refraction and myopia progression remains unproven, but an association does seem to exist[60] and this potential risk factor should not be discarded.

1.3.3.2. Parental Myopia

Several studies investigating the influence of parental myopia in the development of myopia in children have found significant associations between them both[61–63]. Children with a less hyperopic refraction and at least one myopic parent are at greater risk of becoming myopic[62,64,65]. Accordingly, parental myopia seems to be linked with a more negative refraction and a greater axial length in their offspring[61,64]. In myopic children, those who are younger and have a more negative refraction and two myopic parents are at higher risk of developing high myopia[66].

Genetic studies have found an association between genes, ocular refraction and biometry[67], and several genes have been identified in association with high myopia[68]. However, the fact that families share both the same environment and culture is a confounder for the effect of genetic traits in the development of myopia[69]. Accordingly, environmental and behavioural factors should both be accounted for in the study of the risk factors for myopia.

1.3.3.3. Near Work

A larger amount of time spent in near work activities has been positively associated with a higher risk for myopia development in Turkish[70] and Taiwanese children[71]. The number of books read per week as a measure of near work activity was found to be associated with high myopia and early onset myopia in Asian children[72]. Even so, due to the young age of the participants and the fact that their myopia is of early onset, this association may not be a risk factor. Instead, it is likely influenced by environmental and/or genetic factors[72]. Short reading distance and reading for more than 30 minutes straight have been positively correlated with the development of myopia in Australian children, rather than total time spent reading[73].

In another study, near work activities were significantly, although weakly, associated with myopia development in American children of several ethnicities. Instead, parental myopia had a much larger effect, along with others factors such as sports practice and academic performance by a smaller degree. This does not support a truly significant effect of near work activities in myopia development, but suggests that there are several factors at play[74].

In contrast, a study involving rural Chinese children has shown no association between time spent in near work activities and myopia development[75]. In conclusion, the effect of near work activities on myopia remains unclear, but it should be considered along with genetic, familiar and other environmental factors.

1.3.3.4. Time Spent Outdoors

Studies show that children who spend more time in outdoor activities are at a lower risk of developing myopia[76,77]. Even in children who spend a long time in near work activities, those who spend more time outdoors are less likely to develop myopia. Outdoor sports practice seems to be correlated with a lower myopia development, but no association was found between indoor sports and myopia[78]. Also, time outdoors has a more significant effect in comparison to sports practice, when considered separately[79]. Therefore, time spent outdoors rather than sports practice seems to protect against the development of myopia.

Time spent outdoors influences several biological mechanisms that may be responsible for this protective effect. Dopamine light-stimulated release is influenced by time spent outdoors, and

seems to prevent excessive eye growth[80]. Thus, high ambient light levels seem to prevent eye growth, as they promote dopamine release in the retina [81]. Also, higher light intensity may increase the depth of field and decrease blur[78]. Despite all this, time spent outdoors does not seem to prevent myopia progression[82,83], so further studies are needed.

1.3.4. The Myopic Retina

1.3.4.1. Cone Photoreceptor Packing Density

Due to the retinal stretching caused by the increasing axial length in myopic eyes, cone spacing is expected to be wider and cone packing density is expected to decrease[20]. Consequently, the variation of the density of the human cones with axial length and refractive error has been recently studied in vivo using AOSLO. The eyes of healthy young adults were shown to have a significant negative correlation between axial length and refractive error[21,22]. Cone packing density was found to be significantly lower in moderate-to-high myopes than in emmetropes and low myopes[20,22,84]. The cone packing density was also found to decrease with increasing eccentricity and axial length in these subjects[20,84,85].

Factors such as gender, ethnicity and ocular dominance do not seem to influence cone density[85]. Age, however, has a less evident effect. Some studies have failed to find an association between cone density and age[85,86] although others have found that cone density significantly decreases in the central fovea in older subjects in comparison with younger ones[87,88].

1.3.4.2. Retinal Function

There are several ways to measure retinal function, ranging from interference fringes, contrast sensitivity and spatial summation tasks to electroretinography.

Coletta & Watson[89] studied how myopia affects visual acuity with interference fringes in young adults. Visual acuity was not to significantly affected when optical factors were corrected, but a significant decrease in retinal acuity was found with increasing myopia in the fovea and at 10° eccentricity. This suggests that the magnification of the retinal image due to the excessive axial length compensates the effect of the wider space between retinal cells in high myopes.

There also seems to be some degree of contrast sensitivity loss in high spatial frequencies in high myopes, especially when wearing spectacles in comparison to contact lenses, which may be an indicator of loss of visual function prior to pathological changes of the fundus[90]. The use of contact lenses may improve the contrast sensitivity function due to the increase in the size of the image projected at the retina.

Studies involving spatial summation tasks that aimed to assess retinal integrity and visual performance of highly myopic eyes have observed increased critical areas for myopic subjects, when compared to emmetropic subjects[45,91]. This points to losses of visual function in these subjects, due to a loss of sensitivity of either the photoreceptors or the post-receptoral neurons (ganglion cells) in the enlarged eye[45,91].

Other studies have investigated changes in retinal function of young healthy adults, ranging from emmetropes to high myopes, using multifocal electroretinography (mERG). Retinal responses were found to decrease significantly with increasing myopia[92,93].These results suggest a cone loss function due to the morphological changes that are produced by the increment of the axial length in the myopic eye[92,93].

In the same way, when studying the relationship between retinal structure and function in highly myopic young subjects, Koh and collaborators[94] found decreased amplitudes in full-field electroretinography (ffERG) results, but normal outer macula and retinal nerve fibre layer thickness, meaning that functional changes precede structural changes in these subjects.

The previous studies point to the same conclusion, that retinal function may be compromised due to the excessive elongation of the myopic eye, which may affect the function of photoreceptors and post-receptoral processes before any structural or pathological changes are present or visible.

1.3.5. Wavefront Aberrations and Myopia

Wavefront aberrations result from light scattering induced by the ocular media. They can have an effect in the retinal image and impact the quality of vision. Wavefront aberrations are often expressed in Zernike coefficients, which are distributed in several magnitude orders. First order aberrations usually have the highest values, and tend to decrease as the order of the coefficients increase. Second order aberrations include the sphero-cylinder aberrations and can be corrected

with an optical prescription. Terms higher than the second order are known as the higher order aberrations (HOAs). The sum of the HOAs values are approximately zero, and the highest contributions come from the fourth order spherical aberration and third order coma. These are unable to be compensated by the usual optical prescription means[95,96].

Several studies have been conducted to see if HOAs differ between myopes and non-myopes, and although some early studies did find that myopes had higher HOAs, methodological limitations constrain these findings, and other more recent studies with more objective methods found none (for a review, see Charman[95]). So, there is a lack of evidence supporting the role of wavefront aberrations in the development of myopia at the present time, but it is believed that higher levels of HOAs may be found in some stages of the process, as a consequence of the eye actively shifting its refraction[95].

1.3.6. Chromatic Signals and Myopia

Short-wavelengths have a shorter focal length than long-wavelengths due to the eye's optical components chromatic aberration. This phenomenon blurs part of the retinal image decomposing the image into blurred coloured components[97]. In a black and white edge, the edge will have a fringe of the colour of the blurred farthest wavelength. The fringe will be red when there is a hyperopic defocus (blue is focused and red and green are blurred). And the fringe will be blue in a myopic defocus (red is focused and green and blue are blurred)[98]. Consequently, when a hyperopic defocus of the longer-wavelength light is present, the eye will use the signal of the most focused colour (the blue one) and grow to try to compensate it[99]. It was also found that long-wavelength light seems to induce myopia in some mammals. Guinea-pigs exposed to green light showed a suppression of melatonin production (regulator of eye growth) and suffered a myopic-shift in their refraction, by vitreous chamber and overall axial elongation[100]. On the contrary, chicks exposed to blue light by a larger amount of time than other chicks maintained their refraction and seemed to enjoy a protective effect[101].

In humans, there also seems to be a relationship between colour vision and myopia development. A study involving Chinese teenage students found that students with normal colour vision were more myopic and had more elongated eyes than students with protan and deutan

defects[102]. Furthermore, other studies found that myopic subjects are more sensitive to long-wavelength stimuli than emmetropic ones, when the myopia is effectively stablished[97,103].

1.3.7. Pathologic Myopia

The stress induced by the excessive stretching of the eye may causes several degenerative changes in highly myopic eyes, leading to severe complications that include vision loss[104].The highly myopic eye becomes deformed in shape, instead of the spherical shape of an emmetropic eye or the prolate shape of low or moderate myopes, and its scleral and choroidal thickness tends to decrease[105]. These changes are associated to posterior staphyloma, chorioretinal atrophy and choroidal neovascularization, lesions of pathologic myopia[104,105]. Since almost 1 billion people will be at risk of suffering myopia-related ocular complications and vision loss in the near future[51], instruments that allow for their early detection and monitoring are of great importance.

2. HYPOTHESIS AND AIMS OF THE STUDY

2.1. Problem Formulation

Recent findings have shown that the cone photoreceptor density in myopic eyes differs from non-myopic, being lower in the first ones. High myopic eyes have also been shown to suffer significantly functional losses due to the pressure of an excessive axial length. Accordingly, it is possible that the colour discrimination of high myopes may be limited when compared with non-myopes. High myopes are at greater risk to develop pathological fundus changes associated to pathological myopia, including cone loss. Therefore, it is important to determine when the functional losses become significant and to be able to monitor them before they turn into structural losses. The determination of the chromatic discrimination thresholds may be relevant in the assessment of such losses.

2.2. Hypothesis

1. The axial length and refractive error are related to the chromatic discrimination thresholds;
2. Subjects with high myopia (< -6 D or an axial length > 25 mm) have significantly different chromatic discrimination thresholds in comparison to the remaining subjects.

2.3. Aims

The main goals of this thesis are:

1. To assess the differences in colour perception between myopic and non-myopic subjects; and
2. To evaluate these differences as a possible tool for the detection and monitoring of pathological myopia.

3. MATERIAL AND METHODS

3.1. Study Design

Little is known about the correlation between the length of myopic eyes, their refractive power and its impact on the colour vision discrimination.

Being a preliminary study, the primary goals of this work were to compare the differences between the colour discrimination thresholds of myopes and non-myopes observers and relate it with their refractive and axial length status. It was divided in two major parts: first, the objective refractive error and the eye axial length were measured, and, second, the chromatic discrimination thresholds were determined.

This study took place at the Clinical and Experimental Optometry Research Lab (CEORLab) and the Colour Science Lab at the University of Minho (Braga, Portugal). All the instruments used in this study were available at the CEORLab (part 1) and at the Colour Science Lab (part 2). All participants signed a Consent Form once the purpose and procedures of the study were fully explained to them (appendix 1). All the experimental procedures performed were non-invasive.

3.2. Participants and Sample Size

Participants were recruited from the academic community. All participants had to be 18 to 29 years-old and generally healthy. Inclusion criteria also required ocular media transparency, the absence of pathological changes of the fundus, no history of ocular complications and/or surgery and normal intraocular pressure.

At first, 43 participants were enrolled in the study, but one of the participants had a vitrectomy due to a retinal detachment at a young age and had to be excluded. All the other participants met the inclusion criteria, and a total of 42 subjects completed the study.

3.3. Experimental Procedure

All measures were taken between the months of May and August of 2016. First, the participants were asked about their ocular history, general health history and family health history,

and afterwards the refractive error and visual acuity were determined, along with the ocular health assessment and the axial length measurement (appendix 2). If the participants met the inclusion criteria, they would then perform the chromatic thresholds determination tests.

3.3.1. Refractive Error

The habitual eyeglass or contact lens prescription of the participants was recorded, using the focimeter or the original blisters information, respectively. The refractive error was also objectively determined by the Grand Seiko WAM-5500 open field refractometer (Grand Seiko Co. Ltd., Hiroshima Japan). Five measures were taken for each eye and their mean values were recorded, after ensuring that the participants were comfortably seated and had their head and chin pressed against the rests.

The mean sphere (S), negative cylinder (C') and cylindrical axis (α) were converted to power vectors (M, J_0 and J_{45}) for the statistical analysis of the refractive data. The M component expresses the mean spherical equivalent, and J_0 and J_{45} express the vertical and oblique astigmatism components, respectively. J_0 is positive for with-the-rule astigmatism and negative for against-the-rule astigmatism. J_{45} is positive for 45° and negative for 135°[106].

$$M = S + \left(C'/_2\right)$$

$$J_0 = -\left(C'/_2\right)\cos 2\alpha$$

$$J_{45} = -\left(C'/_2\right)\sin 2\alpha$$

3.3.2. Visual Acuity

Visual acuity was measured with the habitual prescription and using the Logarithmic Visual Acuity Chart ETDRS distance chart (Precision Vision, La Salle IL, USA) at 4 meters, as recommended by the manufacturer. The ETDRS distance chart used consists of 14 lines with 5 letters each, that are arranged in a geometric progression and printed in high contrast. Each letter has a score value of 0.02 log units. The chart measures visual acuities between 1.0 LogMAR units (0.1 in decimal scale) and -0.3 LogMAR units (2.0 in decimal scale), and the line of 0.0 LogMAR matches 1.0 in decimal scale. Measures were monocular and binocular and room luminance was

at a photopic level of 85 cd.m^{-2}. The score value for each eye was recorded and used as the metric of the visual acuity.

3.3.3. Ocular Health Assessment

Ocular health was assessed through slit lamp observation, tonometry and retinography, and an optometric assessment was written down in each participant's clinical chart. Throughout the procedure, it was ensured that the participants were comfortably seated in front of each instrument, with their chin and/or forehead pressed against the chinrest and they were instructed to look at the different fixation targets or relevant directions.

Slit lamp observation was performed in order to evaluate the ocular media transparency and to guarantee that there were no opacities that could impact the colour vision of the participants.

The Cobra non-mydriatic fundus camera (C.S.O. SRL, Firenze, Italy) was used for retinal imaging. The participants were told to look at the orange fixation target and warned that there would be a flash for the image acquisition. An optometric decision was then made based on the image acquired. A normal fundus, even a characteristically myopic fundus, was required to ensure a normal function of the retina.

Tonometry was performed with Ocular Response Analyzer (ORA) (Reichert Inc, Buffalo NY, USA). The ORA tonometer measures the Goldmann-correlated intraocular pressure (IOPg), the corneal compensated intraocular pressure (IOPcc), which is compensated for the corneal biomechanical properties by measuring the corneal resistance factor (CRF) and the corneal hysteresis (CH) (also in the output). The participants were instructed to look at the green fixation target, which was surrounded by four red lights and to open their eyes wide. Four measures were taken for each eye and the mean values were estimated and recorded. A normal intraocular pressure was required to exclude high intraocular pressure as a source of retinal ganglion cell death.

3.3.4. Wavefront Aberrometry

Wavefront aberrometry was measured using the IRx3 aberrometer (ImaginEyes, France). Three measures were made for each eye in scotopic conditions without induced mydriasis. The

participants were instructed to look at the fixation target and to blink three times before the measure was taken. The mean values of the root mean squares (RMS) from the third to the sixth order, the HOAs and the coma and spherical aberrations were determined for a 5-mm pupil.

3.3.5. Axial Length

The axial length was measured with the ZEISS IOLMaster Optical Biometer (Carl Zeiss, Jena, Germany). This instrument measures the signal produced by the interference between the light reflected by the tear film and that reflected by the retinal pigmentary epithelium along the visual axis, yielding the axial distance in millimetres. The participants were instructed to look at the fixation target and to blink three times. Five measures were taken for each eye to obtain the mean axial length.

3.3.6. Chromatic Thresholds Determination

After checking for the normal ocular health and the determination of the refractive error and axial length, the participants performed two colour vision tests: The Cambridge Colour Test (CCT) (version 2.31, Cambridge Research Systems Ltd.) and the Colour Assessment and Diagnosis Test (CAD) (version 2.3.1.1, City Occupational Ltd.).

Each test ran for about ten minutes and was repeated twice, with small breaks between tests so that the participant could rest. While performing the tests, the participants wore a trial frame with the habitual prescription (if needed) to eliminate the influence of different filters and treatments of their personal refractive correction. All tests were binocular so they would be completed in only one visit. All tests were performed in a dark room in order to minimize distraction and potential chromatic clues.

3.3.6.1. Cambridge Colour Test

Each plate of the CCT was displayed for 4 seconds and the participants had to identify the orientation of the gap, out of four possible directions (up, down, left and right), by responding on a keypad. The gap should subtend 1° of visual angle, so the participants were seated at 3 meters

from the display. When unable to identify the gap direction, the participants were instructed not to answer and wait out the 4 seconds. But, when in doubt, they were encouraged to answer the suspected direction. Luminance test range was set to vary in six steps between 8 and 15 cd.m^{-2}. The mean thresholds for 20 colour space vectors with a set chromaticity of (x = 0.1947, y = 0.4639) that corresponded to the background CIE-*x, y* 1931 coordinates, were plotted and an ellipse comprising the chromatic thresholds was obtained. The test was displayed in a Sony Triniton GDM-FW900 monitor previously calibrated, with a spatial resolution of 1264x790 and a frame rate of 100 Hz.

3.3.6.2. Colour Assessment and Diagnosis Test

The CAD test uses a 2.9° chromatic square that moves at a constant speed of ~4°/s in four possible diagonal directions. The square is inserted in a 3.3° larger square dynamic background[38,39].

Testing display was a NEC MultiSync PA 241w (NEC67D1) TFT monitor, with a spatial resolution of 1920x1200 and a frame rate of 60 Hz, with background luminance set to 24 cd.m^{-2} and background CIE chromaticity coordinates (x = 0.305, y = 0.323). The participants were comfortably seated at 1.40 meters of the display in order to respect the intended visual angles. After instructed, the participants had to identify the direction in which the chromatic square stimulus had moved, by responding in a remote numeric keypad with evidenced diagonals. The test is forced-choice, so they were encouraged to respond randomly when failing to detect the chromatic stimulus.

3.4. Statistical Analysis

Statistical Analysis was performed with IBM SPSS Statistics software version 23.0 (SPSS Inc., Chicago IL, USA). The descriptive data were presented in terms of mean and standard deviation. The data of the eye with best visual acuity obtained in the first part of this study were used for the analysis of colour vision tests results, since this is the eye that mainly contributes for the binocular vision information.

The colour spaces of both colour vision tests are different, which means that the same coordinates have different positions. Therefore, CAD chromatic thresholds were transformed from *x, y* into *u', v'* coordinates for comparison with the CCT chromatic thresholds. The chromaticity coordinates were converted into discrimination thresholds by computing the Euclidean distance between them and the colour of the background for each hue. The chromatic discrimination thresholds of both tests were then compared by hue (or vector under analysis) to assess the sensitivity of the tests in detecting changes in colour vision associated with myopia progression. Based on the orientation of the vectors of the tested directions, the thresholds were grouped by their corresponding hues, red (R), green (G), yellow (Y) and blue (B), and by quadrants (Q) only for the CCT (Table 1).

Table 1. Chromatic thresholds of the CAD test and the CCT grouped into hues and quadrants.

Hue	CAD CIE x, y (°)	CAD CIE u', v' (°)	CCT Q vectors	CCT Q CIE u', v' (°)	CCT vectors	CCT CIE u', v' (°)
R	320-355	360	19-3	324-36	20-2	342-18
Y	60-64	90	4-8	54-126	5-7	72-108
G	140-175	180	9-13	144-216	10-12	162-198
B	240-244	270	14-18	234-306	15-17	252-288

For the CAD test, R included the 6 vectors between 320 and 355°, Y included the 2 vectors between 60 and 64°, G included the 6 vectors between 140 and 175°, and B included the 2 vectors between 240 and 244°.

For the CCT, the vectors were first grouped by quadrants. The R quadrant (Q1) included the vectors 19-20, 1-3, the Y quadrant (Q2) included the vectors 4-8, the G quadrant (Q3) included the vectors 9-13 and the B quadrant (Q4) included the vectors 14-18. In order to reduce the noise of the frontier values between quadrants, CCT mean chromatic discrimination thresholds for each hue were determined including only vectors 1, 2 and 20 for R, 10-12 for G, 5-7 for Y and 15-17 for B (for detailed description of the vectors used, please refer to appendix 4).

An exploratory analysis of the data dispersion was performed to exclude eventual outliers. The normality and homogeneity of the data was evaluated using the Shapiro-Wilk ($N < 50$) and Levene tests, respectively. If the statistical significance (p-value) was less than 0.05, the null hypothesis would be rejected, which meant that there were significant differences in the distribution of the sample compared to a sample with normal distribution.

Correlations were determined for the variables with the Spearman's rank correlation. The correlations were considered strong if > 0.80, moderately strong if between 0.5 and 0.8, fair if between 0.3 and 0.5 and poor if < 0.30.

The sample size did not warrant the normality of the data, requiring the use of non-parametric tests.

Participants were divided in three and four different groups for the two independent variables, axial length and refractive error, respectively. In accordance to their axial length, the groups were: small (≤ 23.50mm; N = 12), medium (23.51 to 25.00 mm; N = 17), and long eyes (>25.00 mm; N = 13), corresponding to non-, low-to-moderate and high myopes. In accordance to their objective refraction, the groups were: non-myopes (≥ -0.50 D; N = 14), low myopes (-0.51 D to -3.00 D; N = 11), moderate myopes (-3.01 D to -6.00 D; N = 9) and high myopes (< -6 D; N = 8). Kruskal-Wallis and Mann-Whitney post hoc tests were used to compare the chromatic discrimination thresholds of the groups.

Statistical significance was set at $\alpha = 0.05$.

4. RESULTS

4.1. Sample Demographics

The characteristics of the subjects used in this study are summarized below. Table 2 includes the parameters that were measured in the first part of the study expressed in mean and standard deviation. Forty-two participants were included in this study, of which 35 were females and 7 were males.

Table 2. Subjects' demographics. AL = axial length; M = mean spherical equivalent; J0 = vertical astigmatism component; J45 = oblique astigmatism component; IOPcc = corneal compensated intraocular pressure; IOPg = Goldmann correlated intraocular pressure; CRF = corneal resistance factor; CH = corneal hysteresis; RMS = root mean square; HOA = higher order aberrations; SD = standard deviation.

Parameter		Mean±SD
	Age (years)	22.9±2.1
Refraction	AL (mm)	24.34±1.30
	M (D)	-2.68±3.02
	J0 (D)	+0.27±0.35
	J45 (D)	+0.03±0.16
	Visual acuity (LogMAR)	-0.07±0.10
Corneal biomechanics	IOPcc (mm Hg)	14.50±2.78
	IOPg (mm Hg)	14.17±3.14
	CRF (mm Hg)	10.23±1.75
	CH (mm Hg)	10.73±1.48
Wavefront aberrations	Third order RMS (μm)	0.171±0.066
	Fourth order RMS (μm)	0.083±0.043
	Fifth order RMS (μm)	0.036±0.015
	Sixth order RMS (μm)	0.030±0.009
	HOA RMS (μm)	0.202±0.066
	Spherical aberration RMS (μm)	0.070±0.054
	Coma aberration RMS (μm)	0.127±0.065

The mean axial length of this population (24.34 ± 1.30 mm) was higher than the axial length of the standard emmetropic eye (22.22 mm). Accordingly, the mean spherical equivalent of the sample was myopic (-2.68 ± 3.02 D), mainly with low with-the-rule astigmatism. Mean visual acuity was below 0.0 LogMAR, which is equivalent to a visual acuity above 20/20, indicating a good visual acuity.

Mean IOP values (14.50 ± 2.78 mm Hg) were lower than 22 mm Hg, and corneal hysteresis and corneal resistance factor were approximately 10 mm Hg. Concerning the mean values of the root mean squares (RMS) of wavefront aberrations, coma and third order aberrations seem to have the larger contribution in mean higher order aberrations (HOAs) than mean spherical and fourth order aberrations. Fifth and sixth order aberrations are the lowest values. Wavefront aberrations decreased the higher the order. The mean values of the RMS were positive, meaning that the wavefront was ahead of the reference sphere for each. Table 3 summarizes the mean values of each higher-order Zernike coefficient of the 42 participants.

Table 3. Mean higher-order Zernike coefficients determined by wavefront sensing. SD = standard deviation.

Parameter	Mean±SD
Z(3,-3) (μm)	-0.065±0.076
Z(3,-1) (μm)	0.070±0.101
Z(3,1) (μm)	-0.001±0.071
Z(3,3) (μm)	0.000±0.061
Z(4,-4) (μm)	0.009±0.028
Z(4,-2) (μm)	0.001±0.019
Z(4,0) (μm)	0.053±0.058
Z(4,2) (μm)	-0.018±0.025
Z(4,4) (μm)	-0.002±0.022
Z(5,-5) (μm)	-0.002±0.017
Z(5,-3) (μm)	0.007±0.016
Z(5,-1) (μm)	0.002±0.020
Z(5,1) (μm)	-0.002±0.013
Z(5,3) (μm)	0.000±0.009
Z(5,5) (μm)	-0.001±0.016
Z(6,-6) (μm)	0.001±0.015
Z(6,-4) (μm)	0.000±0.010
Z(6,-2) (μm)	0.000±0.007
Z(6,0) (μm)	-0.003±0.013
Z(6,2) (μm)	0.005±0.010
Z(6,4) (μm)	0.001±0.012
Z(6,6) (μm)	-0.003±0.013

4.2. Ocular Parameters

There was a strong statistically significant negative correlation between axial length and mean spherical equivalent between the 42 participants (r_s = -0.853, p < 0.001). It was found that with increasing axial length, the myopic refraction also increased.

The correlations between axial length, mean spherical equivalent and other ocular parameters measured in the first part of this study were also determined for the 42 participants (appendix 3). They were not included in this chapter as the results obtained do not denote a particularly strong correlation between the analysed variables, and only the statistically significant correlations are described.

Both axial length and mean spherical equivalent had a statistically significant fair correlation with corneal compensated intraocular pressure (IOPcc) (AL: r_s = 0.359, p-value = 0.019; M: r_s = -0.444, p-value = 0.003). With increasing axial length and myopic refraction (more negative mean spherical equivalent) IOP also increased. The refractive error was fairly correlated with statistical significance with corneal hysteresis. With increasing myopia, corneal hysteresis decreased.

Concerning wavefront aberrations, both axial length and mean spherical equivalent had a statistically significant fair correlation with vertical coma (Z(3,-1): AL r_s = 0.475, p-value = 0.001; M r_s = -0.446, p-value = 0.003) and secondary spherical aberration (Z(6,0): AL r_s = 0.306, p-value = 0.049; M r_s = -0.320, p-value = 0.039). With increasing axial length and myopic refraction (more negative M), the vertical coma and secondary spherical aberration also increased.

4.3. Colour Vision

4.3.1. Corneal Biomechanics and Wavefront Aberrations

Table 4 summarizes the mean chromatic thresholds across all hues that were obtained with the CAD test and the CCT for the 42 participants, and grouped by hue and quadrant. Results are expressed in mean and standard deviation.

Table 4. Chromatic thresholds of CAD test and CCT expressed in mean and standard deviation. R = red; Y = yellow; G = green; B = blue; Q = quadrant; SD = standard deviation.

Parameter	Mean±SD
CAD	0.0056±0.0016
CAD R	0.0048±0.0013
CAD Y	0.0074±0.0023
CAD G	0.0049±0.0016
CAD B	0.0082±0.0025
CCT	0.0053±0.0015
CCT Q1	0.0049±0.0014
CCT Q2	0.0055±0.0015
CCT Q3	0.0049±0.0013
CCT Q4	0.0060±0.0020
CCT R	0.0050±0.0014
CCT Y	0.0054±0.0014
CCT G	0.0050±0.0014
CCT B	0.0058±0.0018

The correlations between the chromatic discrimination thresholds of the CAD test and the CCT with corneal biomechanics and wavefront aberrations for the 42 participants were determined (appendix 3).

Corneal biomechanics had no statistically significant correlation with the chromatic discrimination thresholds, except for IOPcc with the CCT green hue (r_s = -0.304, p-value = 0.050).

Concerning wavefront aberrations, only some HOAs had a statistically significant correlation with the chromatic discrimination thresholds, and mainly in the CAD test. The fourth order RMS had statistically significant positive fair correlations with the mean CAD and all the hues, except for blue (CAD:r_s = 0.305, p-value = 0.050; CAD R: r_s = 0.305, p-value = 0.050; CAD Y: r_s = 0.349, p-value = 0.024; CAD G: r_s = 0.308, p-value = 0.047). The fifth order RMS had statistically significant positive fair correlations with the mean CAD of all hues and the green hue (CAD: r_s = 0.339, p-value = 0.028; CAD G: r_s = 0.436, p-value = 0.004). The sixth order and the sum of HOAs only had a statistically significant positive fair correlation with the red hue (CAD $R_{\text{sixth order}}$: r_s = 0.453, p-value = 0.003; CAD R_{HOA}: r_s = 0.328, p-value = 0.034). The coma aberration RMS also had statistically significant positive fair correlations with the mean CAD and all the hues, except for blue (CAD:r_s = 0.360, p-value = 0.019; CAD R: r_s = 0.333, p-value = 0.031; CAD Y: r_s = 0.328, p-value = 0.034; CAD G: r_s = 0.341, p-value = 0.027).

Only a few Zernike coefficients had a statistically significant fair correlation with the CAD test chromatic discrimination thresholds as well: Z(3,-1) (CAD: r_s = 0.308, p-value = 0.047; CAD R: r_s = 0.315, p-value = 0.042), Z(4,-2) (CAD: r_s = -0.391, p-value = 0.010; CAD G: r_s = -0.369, p-value = 0.016; CAD B: r_s = -0.325, p-value = 0.036), Z(4,0) (CAD Y: r_s = 0.310, p-value = 0.046), Z(6,-6) (CAD:r_s = -0.386, p-value = 0.012; CAD G: r_s = -0.348, p-value = 0.024; CAD B: r_s = -0.431, p-value = 0.004), and finally Z(6,0) (CAD G: r_s = -0.341, p-value = 0.027).

There were no statistically significant correlations between the HOAs RMS and only a few Zernike coefficients had a statistically significant fair correlation with the CCT chromatic discrimination thresholds: Z(4,-2) (CCT: r_s = -0.314, p-value = 0.043; CCT Q3: r_s = -0.372, p-value = 0.015; CCT G: r_s = -0.339, p-value = 0.028), Z(4,4) (CCT Q4: r_s = -0.314, p-value = 0.043; CCT B: r_s = -0.342, p-value = 0.027), Z(6,-6) (CCT: r_s = 0.314, p-value = 0.043; CCT Q3: r_s = 0.374, p-value = 0.015; CCT Q4: r_s = 0.311, p-value = 0.045), Z(6,-4) (CCT G: r_s = 0.306, p-value = 0.049) and finally Z(6,4) (CCT Q4: r_s = -0.320, p-value = 0.039; CCT G: r_s = 0.314, p-value = 0.043; CCT B: r_s = -0.323, p-value = 0.037). This may indicate that these parameters had minor contributions to the chromatic discrimination thresholds.

4.3.2. Sensitivity of Colour Vision Tests

Table 5 summarizes the non-parametric correlations between the results of both tests by hue and quadrant for the 42 participants.

Table 5. Non-parametric correlations between refractive error and chromatic discrimination thresholds grouped by hue and quadrant. R = red; Y = yellow; G = green; B = blue; Q = quadrant; r_s = Spearman correlation coefficient; * statistically significant at p-value < 0.05.

	CAD	CAD R	CAD Y	CAD G	CAD B
	r_s (p-value)	r_s (p-value)	r_s (p-value)	r_s (p-value)	r_s (p-value)
CCT	0.244 (0.119)	0.096 (0.545)	0.245 (0.118)	0.287 (0.065)	0.212 (0.177)
CCT Q1	0.262 (0.093)	0.197 (0.211)	0.191 (0.225)	**0.323*(0.037)**	0.143 (0.366)
CCT Q2	0.190 (0.228)	-0.004 (0.980)	0.227 (0.147)	0.261 (0.095)	0.173 (0.274)
CCT Q3	0.154 (0.329)	0.031 (0.845)	0.159 (0.314)	0.183 (0.247)	0.152 (0.336)
CCT Q4	0.289 (0.064)	0.122 (0.440)	**0.319*(0.040)**	0.272 (0.081)	0.272 (0.081)
CCT R	0.196 (0.213)	0.147 (0.352)	0.149 (0.347)	0.247 (0.115)	0.115 (0.468)
CCT Y	0.151 (0.341)	-0.041 (0.796)	0.210 (0.183)	0.246 (0.117)	0.129 (0.415)
CCT G	0.151 (0.339)	0.026 (0.870)	0.150 (0.342)	0.219 (0.163)	0.088 (0.578)
CCT B	0.288 (0.064)	0.127 (0.424)	**0.328*(0.034)**	0.251 (0.109)	0.291 (0.061)

In the analysis of the chromatic discrimination thresholds by hue and quadrant, there were no statistically significant correlations between the CAD test and the CCT, except for the yellow hue of the CAD test and the blue hue and quadrant of the CCT, and the green hue of the CAD test and the red quadrant of the CCT. However, these correlations hold no true individual significance since the aim was to compare the same hue under testing between tests.

Table 6 summarizes the correlations between axial length, mean spherical equivalent and the chromatic discrimination thresholds obtained with the CCT and the CAD test for the 42 participants.

Table 6. Non-parametric correlations between axial length, refractive error and the chromatic discrimination thresholds of the CAD test and the CCT, and the chromatic discrimination thresholds grouped by hue and quadrant. AL = axial length; M = mean spherical equivalent; R = red; Y = yellow; G = green; B = blue; Q = quadrant; r_s = Spearman's rank correlation coefficient; * statistically significant at p-value < 0.05; ** statistically significant at p-value < 0.01.

	AL	M
	r_s (p-value)	r_s (p-value)
CAD	**0.367* (0.017)**	**-0.509** (0.001)**
CAD R	**0.379* (0.013)**	**-0.562** (<0.001)**
CAD Y	0.293 (0.060)	**-0.347* (0.024)**
CAD G	0.266 (0.088)	**-0.407** (0.007)**
CAD B	**0.402** (0.008)**	**-0.452** (0.003)**
CCT	-0.155 (0.327)	0.127 (0.423)
CCT Q1	-0.146 (0.355)	0.121 (0.445)
CCT Q2	-0.137 (0.386)	0.127 (0.424)
CCT Q3	-0.234 (0.135)	0.185 (0.242)
CCT Q4	-0.081 (0.612)	0.062 (0.697)
CCT R	-0.145 (0.359)	0.171 (0.279)
CCT Y	-0.123 (0.438)	0.131 (0.408)
CCT G	-0.227 (0.148)	0.236 (0.133)
CCT B	-0.084 (0.596)	0.043 (0.786)

There was a statistically significant fair correlation between axial length and the mean CAD chromatic discrimination threshold of all hues, as well as with the CAD red and blue discrimination thresholds. This means that when the axial length increased, so did these thresholds and the chromatic discrimination worsened for the red and blue regions of the colour space.

There were statistically significant fair and moderately strong correlations between mean spherical equivalent and the mean CAD chromatic discrimination threshold of all hues, and the CAD red, green, yellow and blue discrimination thresholds. The correlation was stronger with the mean chromatic threshold of all hues and the red discrimination threshold. As the myopic refraction increased, so did all the CAD chromatic discrimination thresholds. The chromatic discrimination worsened for all hues with increasing refractive error, but this was more evident for the red region of the colour space. This association was not apparent in the CCT, as there were no statistically significant correlations found. Consequently, the CAD test was more sensitive for detecting chromatic discrimination changes associated with myopia progression.

The following scatterplots summarize the statistically significant correlations between the groups of chromatic discrimination thresholds and the axial length and mean spherical equivalent. A quadratic function was fitted to the data with increase improvements on the coefficient of determination of the fit over a simple linear function fit to the data (Figures 15-19, only significant fits are displayed).

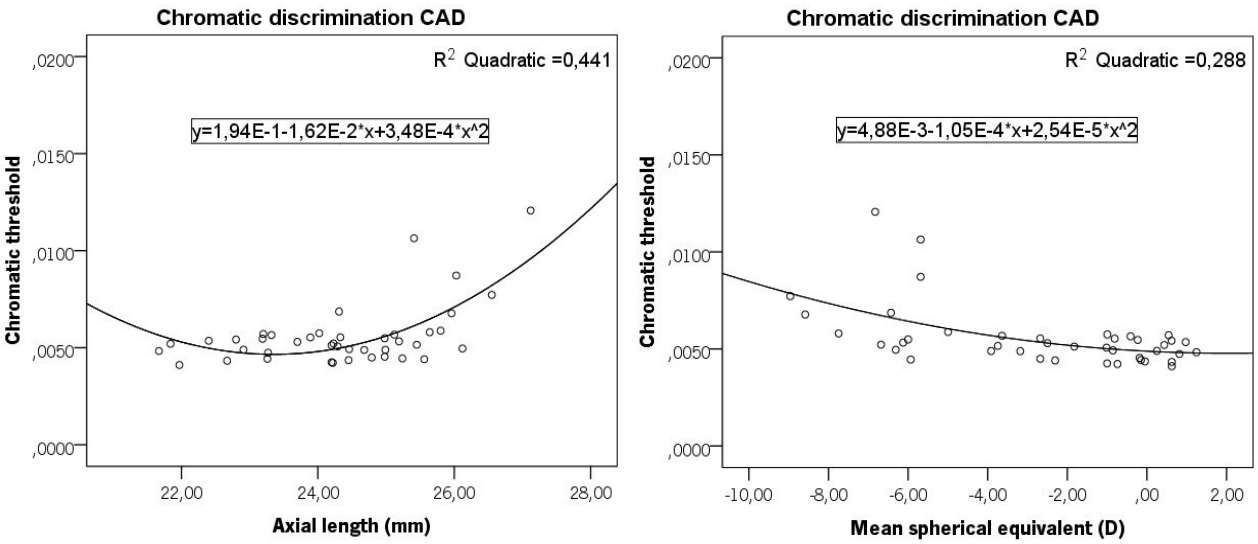

Figure 15. Correlations between the mean CAD chromatic discrimination thresholds and the axial length (left) and mean spherical equivalent (right). R^2 = coefficient of determination.

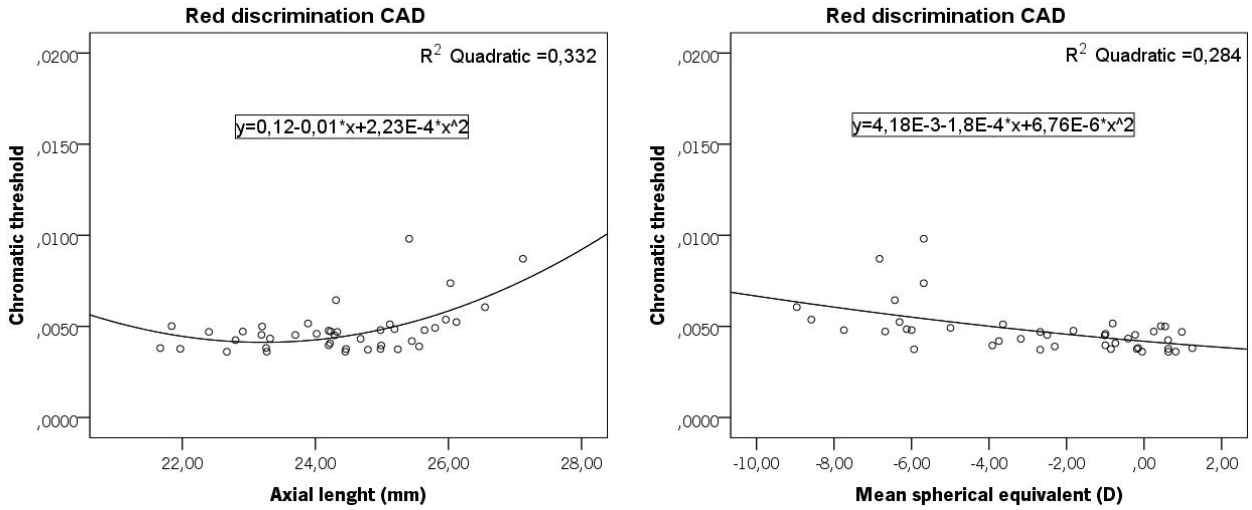

Figure 16. Correlations between the mean CAD chromatic discrimination thresholds for the red hue and the axial length (left) and mean spherical equivalent (right). R^2 = coefficient of determination.

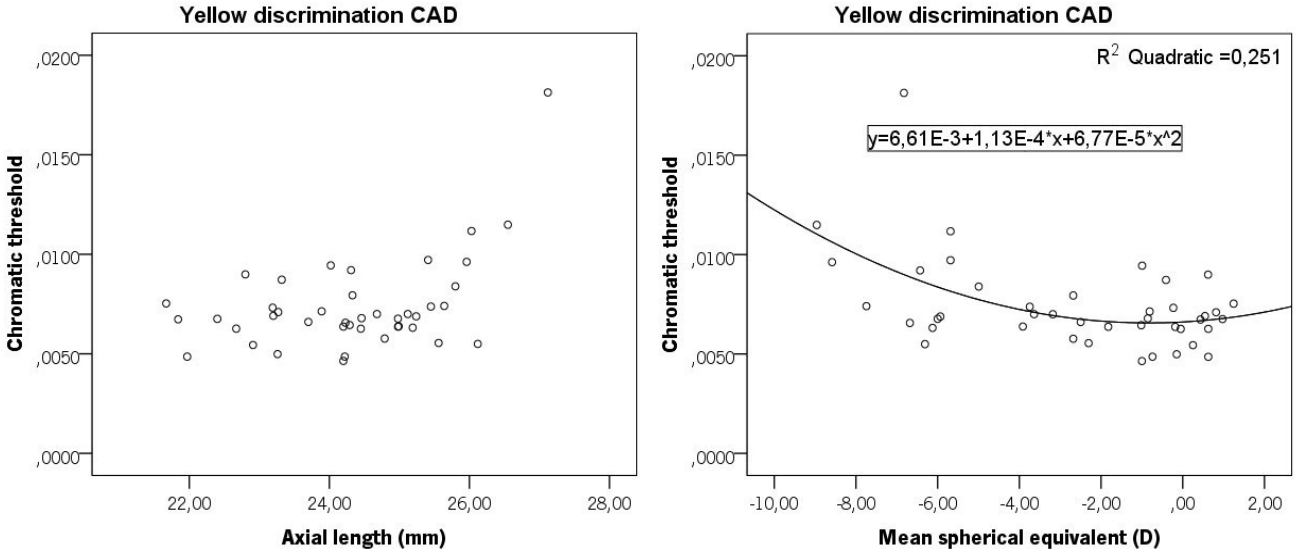

Figure 17. Correlations between the mean CAD chromatic discrimination thresholds for the yellow hue and the axial length (left) and mean spherical equivalent (right). R^2 = coefficient of determination.

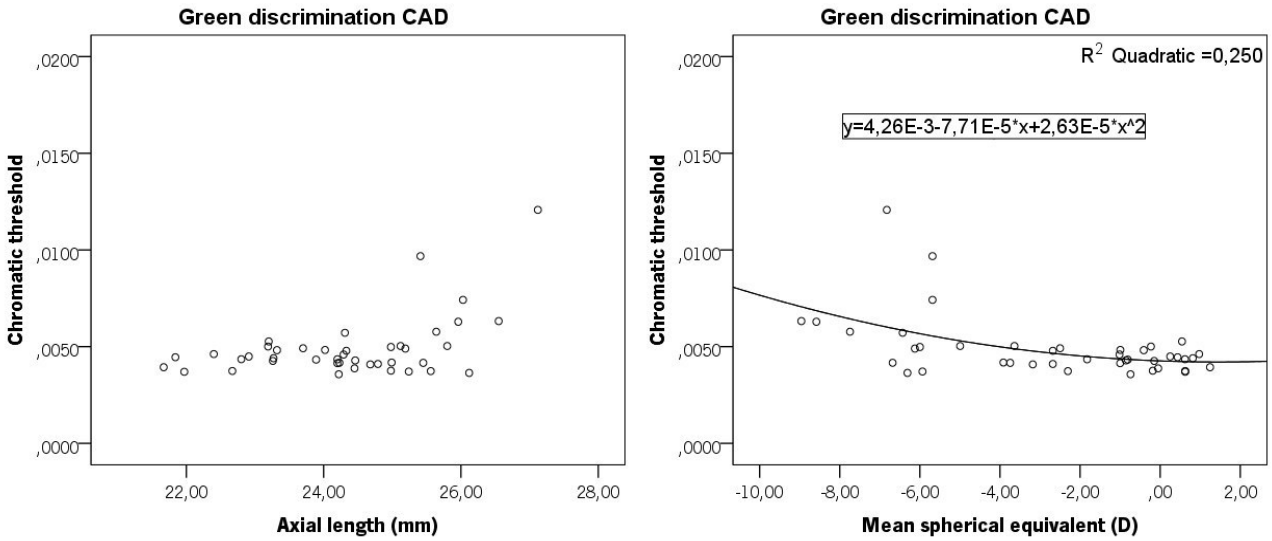

Figure 18. Correlations between the mean CAD chromatic discrimination thresholds for the green hue and the axial length (left) and mean spherical equivalent (right). R^2 = coefficient of determination.

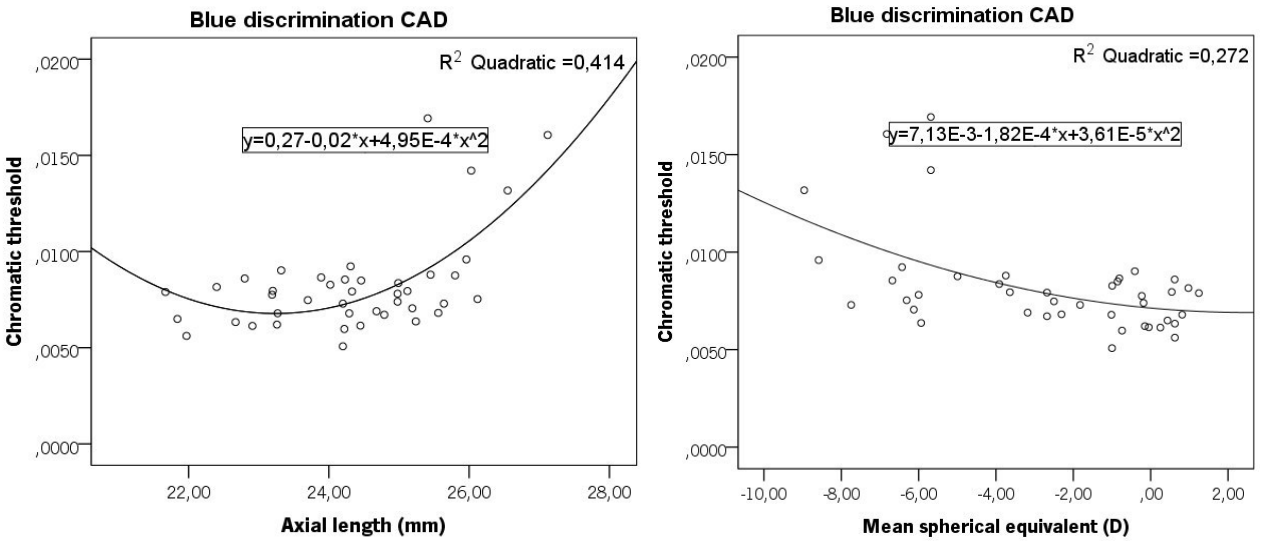

Figure 19. Correlations between the mean CAD chromatic discrimination thresholds for the blue hue and the axial length (left) and mean spherical equivalent (right). R^2 = coefficient of determination.

The chromatic discrimination thresholds are smaller for an axial length of about 23.5 mm and for a mean spherical equivalent of approximately 0 D, i.e., colour discrimination is better in emmetropic eyes than in the others.

4.3.3. Chromatic Discrimination Thresholds and Myopia

Table 7 summarizes the results of the comparative analysis of the chromatic discrimination thresholds of the mean CAD test of all hues and the CAD test hues for axial length and mean spherical equivalent between refractive error groups.

Table 7. Comparative analysis of chromatic discrimination thresholds of the CAD test and the CAD test hues for axial length and mean spherical equivalent between refractive error groups. AL = axial length; M = mean spherical equivalent; non = non-myopes; low = low myopes; moderate = moderate myopes; high = high myopes. SD = standard deviation; R = red; Y = yellow; G = green; B = blue; * = statistically significant for p-value <0.05; ** = statistically significant for p-value <0.01.

Myopia degree		CAD		CAD R		CAD Y		CAD G		CAD B	
		Mean±SD	H (p-value)	Mean±SD	H (p-value)	Mean±SD	H (p-value)	Mean±SD	H (p-value)	Mean±SD	H (p-value)
AL	small	0.0050±0.0005	**7.057***	0.0043±0.0005	**8.876***	0.0068±0.0013	5.287	0.0044±0.0005	4.607	0.0072±0.0011	5.934
	medium	0.0051±0.0007	**(0.029)**	0.0044±0.0007	**(0.012)**	0.0067±0.0012	(0.071)	0.0044±0.0005	(0.100)	0.0075±0.0011	(0.051)
	long	**0.0067±0.0024***		**0.0057±0.0018****		0.0088±0.0034		0.0060±0.0025		0.0100±0.0037	
M	non	0.0049±0.0005	**10.571***	0.0042±0.0005	**14.652***	0.0067±0.0012	6.770	0.0043±0.0005	6.366	0.0072±0.0011	**9.842***
	low	0.0050±0.0005	**(0.014)**	0.0043±0.0005	**(0.020)**	0.0065±0.0014	(0.080)	0.0043±0.0004	(0.095)	0.0072±0.0011	**(0.020)**
	moderate	0.0062±0.0021		0.0054±0.0020		0.0079±0.0016		0.0054±0.0020		**0.0096±0.0036***	
	high	**0.0068±0.0023***		**0.0058±0.0013***		0.0093±0.0041		0.0061±0.0026		**0.0098±0.0032***	

Concerning the results of the comparative analysis by axial length, the chromatic discrimination thresholds were significantly higher for longer eyes in the CAD test in general (variable "CAD") than for small (p-value < 0.050) and medium eyes (p-value < 0.050). Specifically, they were significantly higher for long than for small (p < 0.001) and medium eyes (p < 0.050) in the red region of the colour space (CAD R).

Concerning the results of the comparative analysis by mean spherical equivalent, the chromatic discrimination thresholds were significantly higher for moderate myopes than for non-myopes (p-value < 0.050) in the blue region of the colour space (CAD B). The chromatic discrimination thresholds were also significantly higher for high myopes in the CAD test in general (variable "CAD") than for non-myopes (p-value < 0.050) and low myopes (p-value < 0.050). They

were significantly higher for high myopes than for non-myopes ($p < 0.001$) and low myopes ($p < 0.050$), both in the blue and red regions of the colour space (CAD B and CAD R, respectively).

In the comparative analysis of the chromatic discrimination thresholds of the mean CCT of all hues, the CCT quadrants and the CCT hues between refractive error groups for axial length and mean spherical equivalent, there were no statistically significant differences found (appendix 3).

5. DISCUSSION

This study aimed to investigate possible differences in the chromatic discrimination thresholds of a population of myopic and non-myopic young adults. Subsequently, this study aimed to evaluate these differences as a possible tool for the detection and monitoring of pathological myopia. As such, this chapter first discusses the ocular parameters relations and their influence in colour vision and lastly the use of the chromatic discrimination thresholds in assessing retinal functional changes due to myopia progression.

5.1. Ocular Parameters

The population studied was composed by healthy young adults, with normal IOP, normal visual acuity and normal ocular health. Axial length had a strong significant association with myopic refraction, which is in accordance with several previous studies[107–110]. Myopic eyes usually have a longer length than emmetropic eyes[111], which means that the myopic refraction is highly dependent on the elongation of the eye.

Mean IOP was 14.50 ± 2.78 mm Hg, which is similar to the mean values found in other studies that included subjects of the same age range (13.91 to 15.1 mm Hg)[112–114]. IOP had a fair significant association with increasing axial length and myopic refraction. This is in accordance with a study involving young adults ranging from high hyperopes to high myopes that found a significant association between increasing IOP and increasing axial length[112], and a study involving Iranian young adults that found an increase in IOP with increasing myopic refraction[113]. A significant association between increasing IOP and increasing myopic refraction was also found in children[115] and mature adults[116]. On the contrary, another study investigating the IOP of young adults of the COMET cohort did not find significant differences between moderate myopes and other groups of refractive errors[114].

Although IOP has been associated with axial elongation in a study involving young adults that used ORA[117], and in a study involving chicks eyes[118], other studies, however, have lacked to find a significant association between IOP and myopia[119,120]. A study on the relation between IOP, ethnicity and refractive error also lacked to find significant differences in IOP before and after the development of myopia in children, but these differences varied largely among ethnic groups[115]. Only one of the previous studies used ORA, which compensates its measures for corneal

biomechanics properties that may be altered in corneal pathologies[121], while the others mainly used Goldmann's applanation tonometer, so the results of these studies should be interpreted with caution. Still, this raises the possibility that the increasing IOP values with increasing myopia may be associated with the stress caused by the excessive elongation of the eye rather than the other way around. Therefore, the association between IOP myopia remains unclear. The results of this study, although significant, are only fairly associated, and it should be kept in mind that their interpretation is severely limited by the fact that the measures were taken at a single point in time, and not always at the same time of the day, as well as by the small sample size.

Concerning wavefront aberrations, vertical and horizontal coma and spherical aberration were the highest coefficients (Z(3,-1), Z(3,1) and Z(4,0), respectively). Third order and coma aberrations were the highest root mean squares. Coma-like aberrations seem to have the highest contribution in HOAs, followed by spherical aberrations. Wavefront aberrations decreased with increasing order. These results were as expected[95]. Axial length and mean spherical equivalent had a fair significant association of the same magnitude with vertical coma and secondary spherical aberration, otherwise, there were no associations found between these parameters. This is in accordance with other studies. Lombardo and colleagues[21] lacked to find a relation between axial length and HOAs, and no statistically significant differences were found between emmetropic and myopic young adults. Cheng and colleagues[122] also lacked to find an association between refractive error and HOAs, when comparing the eyes of young adults whose refraction ranged from +5.00 to -10.00 D. Atchison and colleagues[91] only found a few significant parameters in lower and higher order aberrations, but mostly no association was found between HOAs and myopia. This is in accordance with the current belief that the impact of HOAs in retinal image quality does not lead to myopia[95].

5.2. Colour Vision

5.2.1. Corneal Biomechanics and Wavefront Aberrations

IOP does not seem to be associated with chromatic discrimination. All the correlations were not significant, except for one, which was a marginal significance of a fair correlation between IOPcc and the green discrimination for CCT. If it was truly significant, more statistical significant differences would likely be found in the other hues or quadrants and in the CAD test.

In the analysis of the relation between HOAs and chromatic discrimination thresholds, there were only some statistically significant results, mainly in the fourth and sixth order coefficients. This may indicate a small influence of HOAs in chromatic discrimination. However, there are two other optical phenomena that affect the quality of the retinal image: diffraction (which depends on the pupil diameter) and dispersion (which causes the light rays to focus at different points)[123]. In this study, the assessment of retinal image quality was made only through monochromatic wavefront aberrations, i.e., only in one wavelength (780 nm), but each wavelength of light is differently affected by the optical components of the eye[123]. It would be interesting to measure the retinal image quality along the EM spectrum, and not just in one wavelength to adequately infer the influence of the optics of the eye in the chromatic discrimination thresholds.

5.2.2. Sensitivity of Colour Vision Tests

There were no significant associations found between the CAD test and the CCT results, except between the yellow discrimination threshold of the CAD test and the blue quadrant and hue discrimination thresholds of the CCT, and between the green discrimination threshold of the CAD test and the red quadrant discrimination threshold of the CCT. Nevertheless, these results are unlikely to have a truly significant relation, since the associations are between hues/quadrants, and not within hues/quadrants. They may just indicate that the threshold associated with one colour in one test has the same magnitude as the other in the other test.

Accordingly, the CAD test seems to have higher sensitivity in detecting minor changes in chromatic discrimination in association with increasing axial length and myopic refraction than the CCT, as the first was the only test with a statistically significant association between these variables. The longer the axial length and the more negative the refraction, the larger the chromatic discrimination thresholds measured with the CAD test, and the worse the chromatic discrimination. Thus, there seems to be a relation between axial length, refractive error and chromatic discrimination. Looking at the dispersion diagrams, the chromatic discrimination thresholds are smaller when the eye has approximately 23.5 mm in axial length and a refractive error of 0 D, or, in other words, is emmetropic. Nevertheless, it is likely that there are other factors at play, since the associations are only fair strength-wise.

Both colour vision tests are currently used in clinical practice, and seem to be useful in detecting changes in colour vision associated with aging[124,125], glaucoma[126], AMD[127], diabetic retinopathy[127–129], Parkinson[130], multiple sclerosis[131], toxicity[132,133] and for the study of hereditary colour vision deficiency[134,135]. However, when using the CCT, some anomalous subjects can obtain normal results, since their chromatic discrimination thresholds fall in the normal range and remain undetected[36]. On the contrary, the CAD test has higher sensitivity in identifying them. It uses a dynamic luminance contrast noise background associated with a coherent-moving coloured stimulus of a recognizable shape[37]. Otherwise, these subjects can detect residual luminance contrast signals available in static luminance, as opposed to normal observers to whom the signals seem to be isoluminant[39,136]. Although the use of dynamic luminous contrast noise does not affect the outcome for a normal subject, it will increase the thresholds to their true extent for anomalous subjects and correctly identify them[37,136]. This way, this method ensures that all the responses are based only in chromatic signals[39]. This seems to agree with the results of this study. There was no true significant association between both tests, and significant differences were found only between the CAD test in relation to axial length and mean spherical equivalent, indicating its higher sensitivity in detecting minor changes in chromatic discrimination.

5.2.3. Chromatic Discrimination Thresholds and Myopia

In the comparative analysis of the chromatic discrimination thresholds between refractive groups there were some significant differences found. High myopes (longer eyes) seem to have larger chromatic discrimination thresholds than non-myopes (small eyes) and low myopes (medium eyes) for the CAD test in general and in the red region of the colour space, both in terms of axial length and of mean spherical equivalent. For the blue region of the colour space, in terms of mean spherical equivalent, not only do high myopes significantly differ from non-myopes and low myopes, but moderate myopes significantly differ from non-myopes as well, and the chromatic discrimination thresholds of the CAD test increase with a more negative refraction. These differences indicate that high myopes and longer eyes seem to have a worse chromatic discrimination than low myopes and non-myopes (smaller eyes).

Myopia seems to be multifactorial in its origin[44]. The correlation between axial length and mean square equivalent found in this study is not perfect, which may reflect to some extent the variation expected in a multifactorial ametropia. Although some risk factors have been identified,

and an interaction between genetics and environment has been recognized[52], it is still unclear what leads to the development of myopia and its progression[44,49]. Nevertheless, colour vision seems to have a role in myopia development. Chromatic hues seem to regulate eye growth due to a different sensitivity of the cone types to wavelengths[99]. Eyes that are more sensitive to long-wavelengths tend to be longer and myopic[97,103], and eyes with red-green colour vision defect tend to be smaller and less myopic[102]. As for the type of defect, hereditary colour vision defects are mostly red-green, and acquired colour vision defects may cause a red-green or a blue-yellow defect[137]. All this raises the question whether increased chromatic discrimination thresholds may be a consequence of an excessively elongated eye or the cause. In this study, the more myopic or longer eyes have increased chromatic discrimination thresholds in the red and blue regions of the colour space. This points to a possible acquired defect but the sample should be larger and include eyes with higher hyperopia degree to allow for a comparison.

The myopic eye has several significant structural differences in terms of its shape[111], peripheral refraction[53–56] and retinal organization of the photoreceptors[20,21] in comparison with normal eyes, and those differences may reflect in its visual performance, or function[94]. Significant differences were found in general and in the red and blue regions of the colour space in high myopes and the correlations between the parameters are mostly only fair, so it is likely that there are other factors influencing the chromatic discrimination of high myopes. Besides, studies on retinal function found that post-receptoral processes are impaired in high myopes[45,91], so it remains unclear what stage of the colour vision information processing is impacted by myopia. Although many important computations of colour vision occur at the early stages of visual information processing, after the retina, several posterior computations occur that are yet to be well established[28].

In this study, some degree of compromised chromatic discrimination has been found in high myopes when using the CAD test, which may imply compromised retinal function. Accordingly, the CAD test seems to be a useful tool in assessing changes in chromatic discrimination due to myopia progression, so further studies with a bigger sample of high myopic subjects are needed.

5.3. Limitations

One of the main limitations of this study was the small sample size, which constrained the results. Some of the participants seemed to have axial myopia, while others seemed to have index/curvature myopia. This might have caused considerable variability in the independent variables in this small sample. A larger sample would decrease the impact of this variability in the data and possibly reinforce the significance of the results. Some relations may have remained undisclosed due to this limitation.

The lack of data of optical quality of the eye was also an important limitation. There are several parameters that would be interesting to measure. Light travels through several media before reaching the retina and suffers several influences, like diffraction and dispersion and not just wavefront aberrations. The refractive power of these media was not determined and its impact on the retinal image quality was also not fully assessed. An individual analysis of the myopic contribution of each refractive power element of the eye would enable a better classification of their impact on the colour perception.

Data collection was made in a single point in time. To properly infer about the chromatic discrimination changes in high myopes, a longitudinal study would be required. There are several forms of myopia and rates of progression, and a more homogeneous and larger sample that included different groups for type (axial or refractive), progression (stable, temporally progressive, permanently progressive) and degree (non, low, moderate, high) would be useful.

Ideally, a subjective examination that provided the correction for the best corrected visual acuity would be performed for each participant. Due to time constraints, all the measures of both parts of the study were taken in a single point in time and with the habitual prescription of the participants to ensure that all the necessary data were collected. Consequently, some of the participants of this study were uncorrected low-hyperopes with good visual acuity, ranging from +0.55 to +1.25 D (N = 7). The potential effect of accommodation on the chromatic discrimination thresholds of the uncorrected hyperopes is possible to be disregarded since their results were normal in both tests. Also, some of the high myopes achieved a visual acuity slightly above 0.0 LogMAR (though all had a habitual prescription less than a year old). A study showed that at least the CCT results are not significant affected by visual acuities lower than 0.86 LogMAR or a refractive blur up to 3 D[138], so the potential effect of an overdue refraction or uncorrected low refractive error

should not have affected in a significant way the chromatic discrimination thresholds of these subjects.

Also, the use of trial frames and lenses to compensate the vision of the ametropic observers had the advantage of equalizing the prescription media across observers. As such, the use of a frame and lens different from the usual may have an impact on the performance of the subjects when performing the colour vision tests. Nevertheless, since the data acquired were based on the mean values of the three runs in both tests, this influence is likely to be reduced as the learning curve to perform the test increased.

6. CONCLUSIONS

In this study, the chromatic discrimination thresholds of non-myopic, low-to-moderately myopic and highly myopic young adults were compared in two different colour vision tests. It was found that axial length and refractive error seem to be associated with the chromatic discrimination thresholds of an individual in the CAD test. Specifically, an increase in axial length and a more myopic refraction seem to be accompanied by increasing chromatic discrimination thresholds in the CAD test, before it is visible in the standard CCT. Furthermore, in the CAD test, subjects with high myopia (< -6 D or an axial length > 25 mm) seem to have significantly larger chromatic discrimination thresholds in comparison to the remaining subjects, which means that their chromatic discrimination is likely to be significantly worse than in normal subjects. On the contrary, there were no significant associations between the chromatic discrimination thresholds obtained with the CCT and axial length and refractive error, which seems to be less sensitive than the CAD test in this case. The CAD test seems to have potential to be a suitable tool for the detection and monitoring of pathologic myopia, as the data reported here did not rule it out completely.

7. FUTURE WORK

For future work, a longitudinal study would be useful. The study should include a larger sample. Separate groups of different types of myopia would turn the sample more homogeneous and might reinforce the results. The inclusion of a larger number of male participants would allow for gender comparisons. A larger range of refractive errors, for instance +5 D to -10D, would also be relevant. And a more profound analysis of the risk factors of myopia by an adequate questionnaire, the classification of myopia in terms of progression and the molecular analysis on the genetics of the sample would also be of interest.

A subjective examination should be performed so that the subjects would be able to achieve the best corrected visual acuity. Regarding the colour vision tests, the sessions should be conducted at the same hour of the day, but in different days, to exclude tiresome and to eliminate potential confounders that may vary along the day, and tests should be monocular and binocular.

Finally, the longitudinal chromatic aberrations should be determined to check for their potential effect in the chromatic discrimination thresholds, and, ideally, imaging of cone photoreceptors would be available, to assess cone ratios and density and rule differences in cone sampling as the reason for different chromatic discrimination.

8. BIBLIOGRAPHY

1. Schwartz SH. *Visual Perception: A Clinical Orientation*. Fourth Edi. New York, NY: McGraw Hill Professional; 2010.

2. Willoughby CE, Ponzin D, Ferrari S, Lobo A, Landau K, Omidi Y. Anatomy and physiology of the human eye: Effects of mucopolysaccharidoses disease on structure and function - a review. *Clin Exp Ophthalmol*. 2010;38:2-11.

3. Roorda A. Human visual system—Image formation. *Encycl Imaging Sci Technol*. 2002;161(1931):539-557.

4. Malhotra A, Minja FJ, Crum A, Burrowes D. Ocular anatomy and cross-sectional imaging of the eye. *Semin Ultrasound, CT MRI*. 2011;32(1):2-13.

5. Sung CH, Chuang JZ. The cell biology of vision. *J Cell Biol*. 2010;190(6):953-963.

6. Swaroop A, Kim D, Forrest D. Transcriptional regulation of photoreceptor development and homeostasis in the mammalian retina. *Nat Rev Neurosci*. 2010;11(8):563-576.

7. Young RW. The renewal of rod and cone outer segments in the rhesus monkey. *J Cell Biol*. 1971;49(2):303-318.

8. Levine MW. *Levine & Shefner's Fundamentals of Sensation and Perception*. Oxford University Press; 2000.

9. Fairchild MD. *Color Appearance Models*. Second Ed. Chichester, UK: Wiley-IS&T; 2005.

10. Purnyn H. The mammalian retina: Structure and blood supply. *Neurophysiology*. 2013;45(3):266-276. doi:10.1007/s11062-013-9365-6.

11. Goldstein. *Sensation and Perception 2013*. 9th ed. Belmont, CA: Cengage Learning; 2013.

12. Bowmaker J, Dartnall H. Visual pigments of rods and cones in a human retina. *J Physiol*. 1980;298:501-511.

13. Curcio CA, Allen KA, Sloan KR, et al. Distribution and morphology of human cone photoreceptors stained with anti-blue opsin. *J Comp Neurol*. 1991;312(4):610-624.

14. Otake S, Gowdy PD, Cicerone CM. The spatial arrangement of L and M cones in the peripheral human retina. *Vision Res*. 2000;40(6):677-693.

15. Roorda A, Williams DR. The arrangement of the three cone classes in the living human eye. *Nature*. 1999;397:520-522.

16. Gowdy PD, Cicerone CM. The spatial arrangement of the L and M cones in the central fovea of the living human eye. *Vision Res*. 1998;38(17):2575-2589.

17. Brainard DH, Calderone JB, Neitz M, Neitz J, Williams DR, Jacobs GH. Functional consequences of the relative numbers of L and M cones. *J Opt Soc Am*. 2000;17(3):607-614.

18. Roorda A, Metha AB, Lennie P, Williams DR. Packing arrangement of the three cone classes in primate retina. *Vision Res*. 2001;41(10-11):1291-1306.

19. Curcio CA, Sloan KR, Kalina RE, Hendrickson AE. Human photoreceptor topography. *J Comp Neurol*. 1990;292:497-523.

20. Chui TYP, Song H, Burns S a. Individual variations in human cone photoreceptor packing density: variations with refractive error. *Invest Ophthalmol Vis Sci*. 2008;49(10):4679-4687.

21. Lombardo M, Serrao S, Ducoli P, Lombardo G. Variations in image optical quality of the eye and the sampling limit of resolution of the cone mosaic with axial length in young adults. *J Cataract Refract Surg*. 2012;38(7):1147-1155.

22. Kitaguchi Y, Bessho K, Yamaguchi T, Nakazawa N, Mihashi T, Fujikado T. In vivo measurements of cone photoreceptor spacing in myopic eyes from images obtained by an adaptive optics fundus camera. *Jpn J Ophthalmol*. 2007;51(6):456-461.

23. Solomon SG, Lennie P. The machinery of colour vision. *Nat Rev Neurosci*. 2007;8(4):276-286.

24. Rushton WAH. Review lecture. Pigments and signals in colour vision. *J Physiol*. 1972;220(3):1P-31P.

25. Nathans J, Thomas D, Hogness D. Molecular genetics of human color vision: the genes

encoding blue, green, and red pigments. *Science (80-).* 1986;232(4747):193-202.

26. Dartnall HJ, Bowmaker JK, Mollon JD. Human visual pigments: microspectrophotometric results from the eyes of seven persons. *Proc R Soc L B Biol Sci*. 1983;220(1218):115-130.

27. Schnapf JL, Kraft TW, Baylor DA. Spectral sensitivity of human cone photoreceptors. *Nature*. 1987;325(6103):439-441.

28. Gegenfurtner KR, Kiper DC. Color vision. *Annu Rev Neurosci*. 2003;26(1):181-206.

29. Birch J. *Diagnosis of Defective Colour Vision*. Oxford University Press; 1993.

30. DeValois R, Abramov I, Jacobs G. Analysis of response patterns of LGN cells. *J Opt Soc Am*. 1966;56(7):966-977.

31. Derrington AM, Krauskopf J, Lennie P. Chromatic mechanisms in lateral geniculate nucleus of Macaque. *J Physiol*. 1984;357:241-265.

32. Palmer SE. *Vision Science: Photons to Phenomenology*. MIT Press; 1999.

33. Hunt RWG, Pointer MR. *Measuring Colour*. Chichester, West Sussex: John Wiley & Sons; 2011.

34. French A, Hons BO, Rose K, et al. The evolution of colour vision testing. *Aust Orthopt J*. 2008;39(2):7-15.

35. Mollon JD, Regan BC. *Cambridge Colour Test Handbook*. London: Cambridge Research Systems; 2000.

36. Regan BC, Reffin JP, Mollon JD. Luminance noise and the rapid-determination of discrimination ellipses in color deficiency. *Vision Res*. 1994;34(10):1279-1299.

37. Barbur JL. “Double-blindsight” revealed through the processing of color and luminance contrast defined motion signals. *Prog Brain Res*. 2004;144:243-259.

38. Barbur JL, Rodriguez-Carmona M, Harlow A. Establishing the statistical limits of “normal” chromatic sensitivity. In: *CIE Expert Symposium, CIE Proceedings 75 Years of the Standard Colorimetric Observer*. Ottawa, Ontario; 2006:1-5.

39. Rodriguez-Carmona ML, Harlow a J, Walker G, Barbur JL. The variability of normal

trichromatic vision and the establishment of the “normal” range. *Proc 10th Congr Interational Colour Assoc*. 2005:0-3.

40. Barbur J, Rodriguez-Carmona M, Evans S, Milburn N. *Minimum Colour Vision Requirements for Professional Flight Crew*. Washington, DC; 2009. https://publicapps.caa.co.uk/docs/33/200904.pdf.

41. Birch J, Rodríguez-Carmona M. Occupational color vision standards: new prospects. *J Opt Soc Am A*. 2014;31(4):A55-A59.

42. Ballard J. Colour-vision safety on track. *Occup Heal Work*. 2013;10(1):20-23.

43. Resnikoff S, Pascolini D, Mariotti SP, Pokharel GP. Global magnitude of visual impairment caused by uncorrected refractive errors in 2004. *Bull World Health Organ*. 2008;86(1):63-70.

44. Morgan IG, Ohno-Matsui K, Saw SM. Myopia. *Lancet*. 2012;379(9827):1739-1748.

45. Jaworski A, Gentle A, Zele AJ, Vingrys AJ, McBrien NA. Altered visual sensitivity in axial high myopia: A local postreceptoral phenomenon? *Investig Ophthalmol Vis Sci*. 2006;47(8):3695-3702.

46. Zejmo M, Formińska-Kapuścik M, Pieczara E, et al. Etiopathogenesis and management of high myopia. Part II. *Med Sci Monit*. 2009;15(11):RA252-A255.

47. Verhoeven VJM, Wong KT, Buitendijk GHS, Hofman A, Vingerling JR, Klaver CCW. Visual consequences of refractive errors in the general population. *Ophthalmology*. 2015;122(1):101-109.

48. Pan CW, Ramamurthy D, Saw SM. Worldwide prevalence and risk factors for myopia. *Ophthalmic Physiol Opt*. 2012;32(1):3-16.

49. Foster PJ, Jiang Y. Epidemiology of myopia. *Eye (Lond)*. 2014;28(2):202-208.

50. Rudnicka AR, Kapetanakis V V, Wathern AK, et al. Global variations and time trends in the prevalence of childhood myopia, a systematic review and quantitative meta-analysis: implications for aetiology and early prevention. *Br J Ophthalmol*. 2016;100:882-890.

51. Holden BA, Fricke TR, Wilson DA, et al. Global prevalence of myopia and high myopia and

temporal trends from 2000 through 2050. *Ophthalmology*. 2016;123(5):1036-1042.

52. Wojciechowski R. Nature and nurture: The complex genetics of myopia and refractive error. *Clin Genet*. 2011;79(4):301-320.

53. Seidemann A, Schaeffel F, Guirao A, Lopez-Gil N, Artal P. Peripheral refractive errors in myopic, emmetropic, and hyperopic young subjects. *J Opt Soc Am A Opt Image Sci Vis*. 2002;19(12):2363-2373.

54. Sng CCA, Lin XY, Gazzard G, et al. Peripheral refraction and refractive error in Singapore Chinese children. *Investig Ophthalmol Vis Sci*. 2011;52(2):1181-1190.

55. Mutti DO, Sholtz RI, Friedman NE, Zadnik K. Peripheral refraction and ocular shape in children. *Investig Ophthalmol Vis Sci*. 2000;41(5):1022-1030.

56. Atchison DA, Pritchard N, Schmid KL. Peripheral refraction along the horizontal and vertical visual fields in myopia. *Vision Res*. 2006;46(8-9):1450-1458.

57. Smith E 3rd, Kee C, Ramamirtham R, Qiao-Grider Y, Hung L. Peripheral vision can influence eye growth and refractive development in infant monkeys. *Invest Ophtalmol Vis Sci*. 2005;46(11):3965-3972.

58. Sng CCA, Lin XY, Gazzard G, et al. Change in peripheral refraction over time in Singapore Chinese children. *Investig Ophthalmol Vis Sci*. 2011;52(11):7880-7887.

59. Faria-Ribeiro M, Queiros A, Lopes-Ferreira D, Jorge J, Meijome JMG. Peripheral refraction and retinal contour in stable and progressive myopia. *Optom Vis Sci*. 2013;90(1):9-15.

60. Radhakrishnan H, Allen PM, Calver RI, et al. Peripheral refractive changes associated with myopia progression. *Investig Ophthalmol Vis Sci*. 2013;54(2):1573-1581.

61. Chua SYL, Ikram MK, Tan CS, et al. Relative contribution of risk factors for early-onset myopia in young Asian children. *Investig Ophthalmol Vis Sci*. 2015;56(13):8101-8107.

62. Xiang F, He M, Morgan IG. The impact of parental myopia on myopia in Chinese children: Population-based evidence. *Optom Vis Sci*. 2012;89(10):1487-1496.

63. Jones LA, Sinnott LT, Mutti DO, Mitchell GL, Moeschberger ML, Zadnik K. Parental history of myopia, sports and outdoor activities, and future myopia. *Investig Ophthalmol Vis Sci*.

2007;48(8):3524-3532.

64. Ip JM, Huynh SC, Robaei D, et al. Ethnic differences in the impact of parental myopia: Findings from a population-based study of 12-year-old Australian children. *Investig Ophthalmol Vis Sci*. 2007;48(6):2520-2528.

65. Zhang X, Qu X, Zhou X. Association between parental myopia and the risk of myopia in a child. *Exp Ther Med*. 2015;9(6):2420-2428.

66. Gwiazda J, Hyman L, Dong LM, et al. Factors associated with high myopia after 7 years of follow-up in the Correction of Myopia Evaluation Trial (COMET) Cohort. *Ophthalmic Epidemiol*. 2007;14(4):230-237.

67. Baird PN, Schäche M, Dirani M. The GEnes in Myopia (GEM) study in understanding the aetiology of refractive errors. *Prog Retin Eye Res*. 2010;29(6):520-542.

68. Hornbeak D, Yung T. Myopia genetics: A review of current research and emerging trends. *Curr Opin Ophthalmol*. 2009;20(5):356-362.

69. Goldschmidt E, Jacobsen N. Genetic and environmental effects on myopia development and progression. *Eye (Lond)*. 2014;28(2):126-133.

70. Hepsen IF, Evereklioglu C, Bayramlar H. The effect of reading and near-work on the development of myopia in emmetropic boys: A prospective, controlled, three-year follow-up study. *Vision Res*. 2001;41(19):2511-2520.

71. Hsu CC, Huang N, Lin PY, et al. Prevalence and risk factors for myopia in second-grade primary school children in Taipei: A population-based study. *J Chinese Med Assoc*. 2015.

72. Saw SM, Chua WH, Hong CY, et al. Nearwork in early-onset myopia. *Investig Ophthalmol Vis Sci*. 2002;43(2):332-339.

73. Ip JM, Saw SM, Rose KA, et al. Role of near work in myopia: Findings in a sample of Australian school children. *Investig Ophthalmol Vis Sci*. 2008;49(7):2903-2910.

74. Mutti DO, Mitchell GL, Moeschberger ML, Jones LA, Zadnik K. Parental myopia, near work, school achievement, and children's refractive error. *Invest Ophtalmol Vis Sci*. 2002;43(12):3633-3640.

75. Lu B, Congdon N, Liu X, et al. Associations between near work, outdoor activity, and myopia among adolescent students in rural China. *Arch Ophthalmol*. 2009;127(2):769-775.

76. French AN, Ashby RS, Morgan IG, Rose KA. Time outdoors and the prevention of myopia. *Exp Eye Res*. 2013;114:58-68.

77. Sherwin JC, Reacher MH, Keogh RH, Khawaja AP, MacKey DA, Foster PJ. The association between time spent outdoors and myopia in children and adolescents: A systematic review and meta-analysis. *Ophthalmology*. 2012;119(10):2141-2151.

78. Rose KA, Morgan IG, Ip J, et al. Outdoor activity reduces the prevalence of myopia in children. *Ophthalmology*. 2008;115(8):1279-1285.

79. Guggenheim JA, Northstone K, McMahon G, et al. Time outdoors and physical activity as predictors of incident myopia in childhood: A prospective cohort study. *Investig Ophthalmol Vis Sci*. 2012;53(6):2856-2865.

80. McCarthy CS, Megaw P, Devadas M, Morgan IG. Dopaminergic agents affect the ability of brief periods of normal vision to prevent form-deprivation myopia. *Exp Eye Res*. 2007;84(1):100-107.

81. Ashby RS, Schaeffel F. The effect of bright light on lens compensation in chicks. *Investig Ophthalmol Vis Sci*. 2010;51(10):5247-5253.

82. Jones-Jordan LA, Sinnott LT, Cotter SA, et al. Time outdoors, visual activity, and myopia progression in juvenile-onset myopes. *Investig Ophthalmol Vis Sci*. 2012;53(11):7169-7175.

83. Wu PC, Tsai CL, Wu HL, Yang YH, Kuo HK. Outdoor activity during class recess reduces myopia onset and progression in school children. *Ophthalmology*. 2013;120(5):1080-1085.

84. Dabir S, Mangalesh S, Schouten J a G, et al. Axial length and cone density as assessed with adaptive optics in myopia. *Indian J Ophthalmol*. 2015;63(5):423.

85. Park SP, Chung JK, Greenstein V, Tsang SH, Chang S. A study of factors affecting the human cone photoreceptor density measured by adaptive optics scanning laser ophthalmoscope. *Exp Eye Res*. 2013;108:1-9.

86. Curcio CA, Millican CL, Allen KA, Kalina RE. Aging of the human photoreceptor mosaic: Evidence for selective vulnerability of rods in central retina. *Investig Ophthalmol Vis Sci*. 1993;34(12):3278-3296.

87. Song H, Chui TYP, Zhong Z, Elsner AE, Burns SA. Variation of cone photoreceptor packing density with retinal eccentricity and age. *Investig Ophthalmol Vis Sci*. 2011;52(10):7376-7384.

88. Panda-Jonas S, Jonas JB, Jakobczyk-Zmija M. Retinal photoreceptor density decreases with age. *Ophthalmology*. 1995;102(12):1853-1859.

89. Coletta NJ, Watson T. Effect of myopia on visual acuity measured with laser interference fringes. *Vision Res*. 2006;46(5):636-651.

90. Liou S, Chiu C. Myopia and contrast sensitivity function. *Curr Eye Res*. 2011;22(2):81-84.

91. Atchison DA, Schmid KL, Pritchard N. Neural and optical limits to visual performance in myopia. *Vision Res*. 2006;46(21):3707-3722.

92. Kawabata H, Adachi-Usami E. Multifocal electroretinogram in myopia. *Investig Ophthalmol Vis Sci*. 1997;38(13):2844-2851.

93. Chan HL, Mohidin N. Variation of multifocal electroretinogram with axial length. *Ophthalmic Physiol Opt*. 2003;23(2):133-140.

94. Koh V, Tan C, Nah G, et al. Correlation of structural and electrophysiological changes in the retina of young high myopes. *Ophthalmic Physiol Opt*. 2014;34(6):658-666.

95. Charman WN. Aberrations and myopia. *Ophthalmic Physiol Opt*. 2005;25(4):285-301.

96. Charman WN. Wavefront aberration of the eye: a review. *Optom Vis Sci*. 1991;68(8):574-583.

97. Rucker FJ, Kruger PB. Cone contributions to signals for accommodation and the relationship to refractive error. *Vision Res*. 2006;46(19):3079-3089.

98. Rucker FJ, Wallman J. Chick eyes compensate for chromatic simulations of hyperopic and myopic defocus: Evidence that the eye uses longitudinal chromatic aberration to guide eye-growth. *Vision Res*. 2009;49(14):1775-1783.

99. Rucker FJ. The role of luminance and chromatic cues in emmetropisation. *Ophthalmic Physiol Opt*. 2013;33(3):196-214.

100. Wang F, Zhou J, Lu Y, Chu R. Effects of 530 nm green light on refractive status, melatonin, MT1 receptor, and melanopsin in the guinea pig. *Curr Eye Res*. 2011;36(2):103-111.

101. Rucker F, Britton S, Spatcher M, Hanowsky S. Blue light protects against temporal frequency sensitive refractive changes. *Investig Ophthalmol Vis Sci*. 2015;56(10):6121-6131.

102. Qian YS, Chu RY, He JC, et al. Incidence of myopia in high school students with and without red-green color vision deficiency. *Investig Ophthalmol Vis Sci*. 2009;50(4):1598-1605.

103. Wienke RE. Refractive error and the green/red ratio. *J Opt Soc Am*. 1960;50:341-342.

104. Wong TY, Ferreira A, Hughes R, Carter G, Mitchell P. Epidemiology and disease burden of pathologic myopia and myopic choroidal neovascularization: An evidence-based systematic review. *Am J Ophthalmol*. 2014;157(1):9-25.e12.

105. Verkicharla PK, Ohno-Matsui K, Saw SM. Current and predicted demographics of high myopia and an update of its associated pathological changes. *Ophthalmic Physiol Opt*. 2015;35(5):465-475.

106. Thibos LN, Wheeler W, Horner D. Power vectors: an application of Fourier analysis to the description and statistical analysis of refractive error. *Optom Vis Sci*. 1997;74(6):367-375.

107. Atchison DA, Thibos LN. Optical models of the human eye. *Clin Exp Optom*. 2016;99(2):99-106.

108. Chau A, Fung K, Pak K, Yap M. Is eye size related to orbit size in human subjects? *Ophthalmic Physiol Opt*. 2004;24(1):35-40.

109. Carney LG, Mainstone JC, Henderson B a. Corneal topography and myopia. *Invest Ophthalmol Vis Sci*. 1997;38(2):311-320.

110. Grosvernor T, Scott R. Comparison of refractive components in youth-onset and early adult-onset myopia. *Optom Vis Sci*. 1991;68(3):204-209.

111. Atchison DA, Jones CE, Schmid KL, et al. Eye shape in emmetropia and myopia. *Investig*

Ophthalmol Vis Sci. 2004;45(10):3380-3386.

112. Tomlinson A, Phillips CI. Applanation tension and axial length of the eyeball. *Br J Ophthalmol*. 1970;54:548-553.

113. Hashemi H, Kashi AH, Fotouhi A, Mohammad K. Distribution of intraocular pressure in healthy Iranian individuals: the Tehran Eye Study. *Br J Ophthalmol*. 2005;69:652-657.

114. Fern KD, Manny RE, Gwiazda J, Hyman L, Weise K, Marsh-tootle W. Intraocular pressure and central corneal thickness in the COMET cohort. *Optom Vis Sci*. 2013;89(8):1225-1234.

115. Manny RE, Mitchell GL, Cotter SA, et al. Intraocular pressure, ethnicity, and refractive error. *Optom Vis Sci*. 2012;88(12):1445-1453.

116. David R, Zangwill LM, Tessler Z, Yassur Y. The correlation between intraocular-pressure and refractive status. *Arch Ophthalmol*. 1985;103(12):1812-1815.

117. Read SA, Collins MJ, Annis-brown T, et al. The short-term influence of elevated intraocular pressure on axial length. *Ophthalmic Physiol Opt*. 2011;31:398-403.

118. Genest R, Chandrashekar N, Irving E. The effect of intraocular pressure on chick eye geometry and its application to myopia. *Acta Bioeng Biomech*. 2012;14(2):3-8.

119. Goss DA, Caffey T. Clinical findings before the onset of myopia in youth: 5. Intraocular pressure. *Optom Vis Sci*. 1999;76(5):286-291.

120. Lee AJ, Saw S-M, Gazzard G, Cheng A, Tan DTH. Intraocular pressure associations with refractive error and axial length in children. *Br J Ophthalmol*. 2004;88:5-7.

121. Devi S. The Ocular Response Analyzer. *J Curr Glaucoma Pract*. 2009;3:24-27.

122. Cheng X, Bradley A, Hong X, Thibos LN. Relationship between refractive error and monochromatic aberrations of the eye. *Optom Vis Sci*. 2003;80(1):43-49.

123. Autrusseau F, Thibos L, Shevell SK. Chromatic and wavefront aberrations: L-, M- and S-cone stimulation with typical and extreme retinal image quality. *Vision Res*. 2011;51(21-22):2282-2294.

124. Paramei G V. Color discrimination across four life decades assessed by the Cambridge

Colour Test. *J Opt Soc Am*. 2012;29(2):A290-A297.

125. Barbur JL, Rodriguez-carmona M. Color vision changes in normal aging. In: Elliott AJ, Fairchild MD, Franklin A, eds. *Handbook of Color Psychology*. UK: Cambridge University Press; 2015:180-196.

126. Castelo-Branco M, Faria P, Forjaz V, Kozak LR, Azevedo H. Simultaneous comparison of relative damage to chromatic pathways in ocular hypertension and glaucoma: Correlation with clinical measures. *Investig Ophthalmol Vis Sci*. 2004;45(2):499-505.

127. O'Neill-Biba M, Sivaprasad S, Rodriguez-Carmona M, Wolf JE, Barbur JL. Loss of chromatic sensitivity in AMD and diabetes: A comparative study. *Ophthalmic Physiol Opt*. 2010;30(5):705-716.

128. Roy MS, Gunkel RD, Podgor MJ. Color vision defects in early diabetic retinopathy. *Arch Ophthalmol*. 1986;104:225-228.

129. Rodgers M, Hodges R, Hawkins J, et al. Colour vision testing for diabetic retinopathy: a systematic review of diagnostic accuracy and economic evaluation. *Health Technol Assess*. 2009;13(60):1-160.

130. Regan BC, Freudenthaler N, Kolle R, Mollon JD, Paulus W. Colour discrimination thresholds in Parkinson's disease: Results obtained with a rapid computer-controlled colour vision test. *Vision Res*. 1998;38(21):3427-3431.

131. Moura ALA, Teixeira RAA, Oiwa NN, et al. Chromatic discrimination losses in multiple sclerosis patients with and without optic neuritis using the Cambridge Colour Test. *Vis Neurosci*. 2008;25:463-468.

132. Ventura DF, Silveira LC, Nishi M, et al. Color vision loss in patients treated with chloroquine. *Arq Bras Oftalmol*. 2003;66:9-15.

133. Ventura DF, Simões AL, Tomaz S, et al. Colour vision and contrast sensitivity losses of mercury intoxicated industry workers in Brazil. *Environ Toxicol Pharmacol*. 2005;19(3):523-529.

134. Konstantakopoulou E, Rodriguez-Carmona M, Barbur JL. Processing of color signals in female carriers of color vision deficiency. *J Vi*. 2012;12(2):1-11.

135. Costa MF, Goulart PRK, Barboni MTS, Ventura DF. Reduced discrimination in the tritanopic confusion line for congenital color deficiency adults. *Front Psychol*. 2016;7:429. doi:10.3389/fpsyg.2016.00429.

136. Birch J, Barbur JL, Harlow AJ. New method based on random luminance masking for measuring isochromatic zones using high resolution colour displays. *Ophthalmic Physiol Opt*. 1992;12(2):133-136.

137. Simunovic MP. Acquired color vision deficiency. *Surv Ophthalmol*. 2016;61(2):132-155.

138. Thyagarajan S, Moradi P, Membrey L, Alistair D, Laidlaw H. Technical note: The effect of refractive blur on colour vision evaluated using the Cambridge Colour Test, the Ishihara Pseudoisochromatic Plates and the Farnsworth Munsell 100 Hue test. *Ophthalmic Physiol Opt*. 2007;27(3):315-319.

Appendix 1

Example of the informed consent presented to and signed by each subject preceding data collection.

Paciente nº: _____

DOCUMENTO DE CONSENTIMENTO INFORMADO

O presente documento visa informá-lo acerca dos objetivos, métodos, benefícios previstos e riscos potenciais inerentes ao estudo para o qual se está a voluntariar, intitulado ***"Miopia e visão das cores, um caso de estudo".***

O presente documento e os procedimentos a que diz respeito estão em conformidade com a "Declaração de Helsínquia" da Associação Médica Mundial (Helsínquia 1964; Tóquio 1975; Veneza 1983; Hong Kong 1989; Somerset West 1996 e Edimburgo 2000, Seul 2008).

A elevada prevalência de alta miopia a nível mundial tem sido encarada como um problema de saúde pública. O comprimento axial excessivo característico da alta miopia pode acarretar complicações oculares, designando-se então por miopia patológica, e pode eventualmente resultar em cegueira. A menor densidade dos fotorreceptores encontrada na retina dos míopes, bem como menores acuidade visual e sensibilidade ao contraste podem sugerir uma limitação na perceção cromática dos míopes em comparação com os não-míopes. Além disso, em casos de doença retiniana, poderá dar-se a perda de cones, fotorreceptores responsáveis pela perceção das cores e pela visão central, sendo importante conseguir determinar quando esta começa a ocorrer de forma significativa e conseguir monitorizá-la.

Este estudo tem como objetivo avaliar as diferenças na perceção cromática entre pacientes míopes e não-míopes e avaliar esta diferença como eventual ferramenta de deteção e monitorização da miopia patológica. Numa primeira fase, será avaliada a saúde ocular e medida a acuidade visual dos participantes e numa segunda fase, efetuar-se-á o exame da visão das cores:

Fase I) Avaliação objetiva da visão e saúde ocular dos participantes, com realização do exame subjetivo e medição da melhor acuidade visual com correção

a) Medição da acuidade visual com correção e da refração por auto-refratómetro
b) Exame do segmento anterior com lâmpada de fenda
c) Avaliação da retina com retinógrafo
d) Determinação do comprimento axial
e) Determinação da pressão intra-ocular
f) Avaliação das aberrações de alta ordem com aberrómetro

Serão excluídos os pacientes com alterações do cristalino, anomalias retinianas e aberrações elevadas. Os exames serão realizados no laboratório de Investigação em Optometria Clínica e Experimental (CEORLab) do Centro de Física da Universidade do Minho em apenas um único momento de avaliação.

Fase II) Avaliação da visão das cores

a) Medida da discriminação cromática com Cambridge Colour Test e CAD

Os exames serão realizados no Laboratório da Cor e serão feitas 3 sessões de cada teste no total com 1h de duração, para obtenção de um valor médio. Os testes de visão das cores serão realizados com armação de prova, de forma a eliminar o efeito de diferentes filtros.

Todos os exames a realizar são não-invasivos.

Declaração de conformidade:

Coloque as iniciais do seu primeiro e último nome à frente de cada afirmação, se concordar com a mesma

Declaro que me foi prestada informação adequada e que me foi igualmente dada a oportunidade de colocar qualquer questão, tendo sida respondida de modo satisfatório.	_____
Entendo que é importante para a minha saúde e para o bom desenvolvimento do projeto seguir as instruções dadas pelo investigador principal.	_____
Compreendo que posso recusar a qualquer momento a continuidade da minha participação no estudo.	_____
Concordo em que os dados obtidos sejam utilizados de forma anónima com os fins científicos ou académicos que a equipa investigadora considerar apropriados.	_____

Braga, _____ de _____ de 2016

O paciente: _____ Assinatura:_____

O investigador: *Dora Nazaré Marques* Assinatura:_____

Este documento é composto por 2 páginas e feito em duplicado: uma via para o/a investigador/a, outra para a pessoa que consente.

APPENDIX 2

Example of the clinical chart used to record the data for each subject of this study.

Ficha clínica

Paciente n.º: _____

Data: _____

Hora:_____

Dados Pessoais

Sexo: _____ Idade: _____

Curso: _____Ano: _____

Historial

Rx OD: _____ 1ª Consulta: _____ Última Consulta: _____

OE: _____ Tipo de Uso: _____

Antecedentes oculares: _____

Saúde Geral: _____

H. F. Ocular: _____

H. F. Saúde: _____

Saúde Ocular

Biomicroscopia: _____

_____

Retinografia: _____

_____

Aberrometria:_____

_____

Tonometria OD:_____

OE:_____

Hora: _____

Medição da acuidade visual e refração

AV Hab OD: _____ AR OD: _____

OE: _____ AO: _____ OE: _____

Biometria

OD:_____OE:_____

Observações

CCT

CAD

APPENDIX 3

The data presented in this Appendix relate the results obtained using the colour vision tests and the ocular parameters measured. The data are highly descriptive and bold values corresponds to significant correlations.

Table A3.1. Non-parametric correlations between corneal biomechanics, wavefront aberrations and axial length and refractive error. AL = axial length; M = mean spherical equivalent; IOPcc = corneal compensated intraocular pressure; IOPg = Goldmann correlated intraocular pressure; CRF = corneal resistance factor; CH = corneal hysteresis; HOA = higher order aberrations; RMS = root mean square; Z = Zernike coefficient; r_s = Spearman's rank correlation coefficient; * statistically significant at p-value < 0.05; ** statistically significant at p-value < 0.01.

		AL	M
		r_s (p-value)	r_s (p-value)
Corneal biomechanics	IOPcc	**0.359* (0.019)**	**-0.444* (0.003)**
	IOPg	0.231 (0.141)	-0.298 (0.055)
	CRF	-0.133 (0.401)	0.102 (0.520)
	CH	-0.289 (0.063)	**0.313* (0.043)**
Wavefront aberrations	Third order RMS	-0.050 (0.753)	0.066 (0.677)
	Fourth order RMS	-0.126 (0.425)	0.058 (0.717)
	Fifth order RMS	0.015 (0.927)	-0.091 (0.564)
	Sixth order RMS	-0.166 (0.293)	-0.060 (0.706)
	HOA RMS	-0.034 (0.829)	0.050 (0.753)
	Spherical aberration RMS	-0.134 (0.397)	0.114 (0.473)
	Coma aberration RMS	0.131 (0.409)	-0.079 (0.620)
	Z(3,-3)	0.209 (0.183)	-0.215 (0.171)
	Z(3,-1)	**0.475** (0.001)**	**-0.446** (0.003)**
	Z(3,1)	0.123 (0.438)	0.034 (0.833)
	Z(3,3)	-0.024(0.882)	0.073 (0.645)
	Z(4,-4)	0.100 (0.530)	-0.004 (0.981)
	Z(4,-2)	-0.045 (0.775)	0.116 (0.464)
	Z(4,0)	-0.214 (0.174)	0.181 (0.252)
	Z(4,2)	0.284 (0.068)	-0.264 (0.091)
	Z(4,4)	-0.259 (0.098)	0.282 (0.070)
	Z(5,-5)	0.035 (0.826)	-0.016 (0.919)
	Z(5,-3)	0.043 (0.788)	0.078 (0.621)
	Z(5,-1)	-0.188 (0.234)	0.288 (0.064)
	Z(5,1)	0.033 (0.835)	0.006 (0.971)
	Z(5,3)	0.021 (0.894)	-0.004 (0.978)
	Z(5,5)	0.010 (0.950)	-0.077 (0.627)
	Z(6,-6)	0.191 (0.227)	-0.237 (0.131)
	Z(6,-4)	-0.252 (0.107)	0.252 (0.107)
	Z(6,-2)	-0.186 (0.239)	0.127 (0.424)
	Z(6,0)	**0.306* (0.049)**	**-0.320* (0.039)**
	Z(6,2)	-0.237 (0.130)	0.268 (0.086)
	Z(6,4)	0.024 (0.878)	-0.104 (0.513)
	Z(6,6)	-0.006 (0.970)	0.103 (0.515)

Table A3.2. Non-parametric correlations between the chromatic discrimination thresholds of the CAD test and wavefront aberrations; HOA = higher order aberrations; RMS = root mean square; Z = Zernike coefficient; r_s = Spearman's rank correlation coefficient. R = red; Y = yellow; G = green; B = blue; * statistically significant at p-value < 0.05; ** statistically significant at p-value < 0.01.

	CAD	CAD R	CAD Y	CAD G	CAD B
	r_s (p-value)	r_s (p-value)	r_s (p-value)	r_s (p-value)	r_s (p-value)
Third order RMS	0.164 (0.298)	0.262 (0.094)	0.130 (0.413)	0.107 (0.499)	0.110 (0.489)
Fourth order RMS	**0.305* (0.050)**	**0.305* (0.050)**	**0.349* (0.024)**	**0.308* (0.047)**	0.213 (0.176)
Fifth order RMS	**0.339* (0.028)**	0.268 (0.087)	0.234 (0.137)	**0.436** (0.004)**	0.167 (0.291)
Sixth order RMS	0.290 (0.063)	**0.453** (0.003)**	0.118 (0.459)	0.281 (0.071)	0.134 (0.398)
HOA RMS	0.235 (0.133)	**0.328* (0.034)**	0.186 (0.238)	0.191 (0.225)	0.136 (0.390)
Spherical aberration RMS	0.190 (0.228)	0.249 (0.111)	0.227 (0.148)	0.192 (0.222)	0.099 (0.531)
Coma aberration RMS	**0.360* (0.019)**	**0.333* (0.031)**	**0.328* (0.034)**	**0.341* (0.027)**	0.272 (0.082)
Z(3,-3)	0.145 (0.359)	0.073 (0.645)	0.126 (0.426)	0.210 (0.183)	0.123 (0.437)
Z(3,-1)	**0.308* (0.047)**	**0.315* (0.042)**	0.294 (0.059)	0.226 (0.151)	0.249 (0.112)
Z(3,1)	-0.105 (0.506)	-0.209 (0.185)	0.130 (0.413)	-0.147 (0.352)	0.058 (0.716)
Z(3,3)	-0.124 (0.436)	-0.035 (0.824)	-0.177 (0.261)	-0.173 (0.273)	-0.231 (0.142)
Z(4,-4)	-0.097 (0.543)	-0.136 (0.392)	-0.002 (0.991)	-0.141 (0.375)	-0.063 (0.694)
Z(4,-2)	**-0.391* (0.010)**	-0.236 (0.133)	-0.275 (0.078)	**-0.369* (0.016)**	**-0.325* (0.036)**
Z(4,0)	0.237 (0.130)	0.248 (0.113)	**0.310* (0.046)**	0.232 (0.140)	0.265 (0.090)
Z(4,2)	-0.118 (0.456)	-0.103 (0.516)	-0.128 (0.419)	-0.044 (0.784)	-0.118 (0.459)
Z(4,4)	0.184 (0.245)	0.095 (0.549)	0.301 (0.053)	0.131 (0.409)	0.104 (0.511)
Z(5,-5)	0.150 (0.341)	0.160 (0.310)	0.169 (0.284)	0.213 (0.175)	0.013 (0.936)
Z(5,-3)	0.026 (0.870)	-0.055 (0.731)	0.005 (0.976)	0.056 (0.725)	0.038 (0.810)
Z(5,-1)	0.048 (0.762)	-0.100 (0.529)	0.138 (0.383)	0.069 (0.665)	0.013 (0935)
Z(5,1)	-0.153 (0.335)	-0.072 (0.651)	-0.149 (0.346)	-0.146 (0.357)	-0.049 (0.759)
Z(5,3)	0.055 (0.731)	0.040 (0.803)	0.040 (0.802)	0.058 (0.716)	0.096 (0.544)
Z(5,5)	0.077 (0.628)	0.056 (0.724)	0.100 (0.527)	0.084 (0.598)	0.150 (0.344)
Z(6,-6)	**0.386* (0.012)**	0.284 (0.068)	0.220 (0.162)	**0.348* (0.024)**	**0.431** (0.004)**
Z(6,-4)	-0.035 (0.825)	-0.086 (0.587)	-0.160 (0.310)	0.085 (0.593)	-0.150 (0.342)
Z(6,-2)	0.030 (0.853)	-0.139 (0.380)	0.097 (0539)	0.033 (0.837)	0.119 (0.455)
Z(6,0)	0.276 (0.077)	0.200 (0.204)	0.219 (0.163)	**0.341* (0.027)**	0.222 (0.158)
Z(6,2)	-0.232 (0.140)	-0.190 (0.227)	-0.168 (0.288)	-0.200 (0.204)	-0.227 (0.148)
Z(6,4)	-0.115 (0.470)	-0.022 (0.889)	-0.249 (0.112)	0.006 (0.968)	-0.127 (0.424)
Z(6,6)	0.090 (0.569)	-0.106 (0.504)	0.302 (0.052)	0.092 (0.561)	0.242 (0.122)

Table A3.3. Non-parametric correlations between the chromatic discrimination thresholds of the CCT, the CCT quadrants and wavefront aberrations; HOA = higher order aberrations; RMS = root mean square; Z = Zernike coefficient; r_s = Spearman's rank correlation coefficient. R = red; Y = yellow; G = green; B = blue; Q = quadrant; * statistically significant at p-value < 0.05.

	CCT	CCT Q1	CCT Q2	CCT Q3	CCT Q4
	r_s (p-value)	r_s (p-value)	r_s (p-value)	r_s (p-value)	r_s (p-value)
Third order RMS	-0.115 (0.469)	-0.052 (0.743)	-0.198 (0.210)	-0.049 (0.756)	-0.084 (0.597)
Fourth order RMS	-0.001 (0.995)	0.035 (0.826)	0.006 (0.970)	-0.139 (0.381)	0.079 (0.620)
Fifth order RMS	0.046 (0.773)	0.092 (0.563)	0.059 (0.708)	-0.027 (0.865)	0.092 (0.564)
Sixth order RMS	0.040 (0.802)	0.063 (0.692)	0.082 (0.607)	-0.038 (0.810)	0.060 (0.705)
HOA RMS	-0.144 (0.364)	-0.062 (0.699)	-0.203 (0.197)	-0.138 (0.385)	-0.083 (0.602)
Spherical aberration RMS	-0.040 (0.803)	0.016 (0.920)	-0.070 (0.661)	-0.135 (0.394)	0.044 (0.783)
Coma aberration RMS	-0.004 (0.981)	0.012 (0.942)	-0.016 (0.921)	-0.022 (0.891)	0.042 (0.790)
Z(3,-3)	0.140 (0.378)	0.096 (0.545)	0.177 (0.263)	0.070 (0.661)	0.166 (0.293)
Z(3,-1)	-0.229 (0.144)	-0.183 (0.246)	-0.232 (0.139)	-0.283 (0.069)	-0.165 (0.295)
Z(3,1)	-0.267 (0.088)	-0.290 (0.063)	-0.198 (0.209)	-0.240 (0.126)	-0.201 (0.203)
Z(3,3)	0.034 (0.831)	0.110 (0.490)	-0.019 (0.903)	0.141 (0.372)	-0.038 (0.812)
Z(4,-4)	-0.128 (0.419)	-0.122 (0.441)	-0.176 (0.265)	-0.125 (0.432)	-0.081 (0.610)
Z(4,-2)	**-0.314* (0.043)**	-0.257 (0.101)	-0.280 (0.072)	**-0.372* (0.015)**	-0.290 (0.063)
Z(4,0)	0.141 (0.371)	0.167 (0.289)	0.159 (0.315)	0.012 (0.942)	0.140 (0.378)
Z(4,2)	-0.245 (0.118)	-0.275 (0.078)	-0.270 (0.084)	-0.183 (0.245)	-0.251 (0.109)
Z(4,4)	0.234 (0.136)	0.235 (0.134)	0.195 (0.217)	0.172 (0.277)	**0.314* (0.043)**
Z(5,-5)	-0.159 (0.313)	-0.119 (0.452)	-0.180 (0.255)	-0.219 (0.164)	-0.076 (0.633)
Z(5,-3)	0.216 (0.170)	0.200 (0.203)	0.218 (0.165)	0.238 (0.129)	0.166 (0.294)
Z(5,-1)	0.163 (0.302)	0.198 (0.210)	0.216 (0.169)	0.082 (0.608)	0.132 (0.404)
Z(5,1)	-0.172 (0.275)	-0.112 (0.481)	-0.160 (0.311)	-0.202 (0.199)	-0.169 (0.283)
Z(5,3)	0.123 (0.436)	0.100 (0.528)	0.149 (0.347)	0.129 (0.417)	0.132 (0.404)
Z(5,5)	0.012 (0.937)	0.014 (0.930)	0.071 (0.657)	-0.031 (0.847)	-0.002 (0.989)
Z(6,-6)	**0.314* (0.043)**	0.253 (0.106)	0.224 (0.154)	**0.374* (0.015)**	**0.311* (0.045)**
Z(6,-4)	0.153 (0.333)	0.150 (0.343)	0.144 (0.362)	0.195 (0.216)	0.102 (0.521)
Z(6,-2)	0.249 (0.112)	0.159 (0.316)	0.291 (0.061)	0.297 (0.056)	0.172 (0.277)
Z(6,0)	-0.109 (0.492)	-0.109 (0.492)	-0.070 (0.661)	-0.069 (0.663)	-0.153 (0.333)
Z(6,2)	0.242 (0.123)	0.206 (0.191)	0.218 (0.165)	0.296 (0.057)	0.240 (0.126)
Z(6,4)	-0.271 (0.082)	-0.239 (0.128)	-0.194 (0.219)	-0.284 (0.068)	**-0.320* (0.039)**
Z(6,6)	0.197 (0.211)	0.096 (0.544)	0.163 (0.303)	0.256 (0.102)	0.209 (0.185)

Table A3.4. Non-parametric correlations between the chromatic discrimination thresholds of the CCT hues and wavefront aberrations; HOA = higher order aberrations; RMS = root mean square; Z = Zernike coefficient; r_s = Spearman's rank correlation coefficient. R = red; Y = yellow; G = green; B = blue; * statistically significant at p-value < 0.05.

	CCT R	CCT Y	CCT G	CCT B
	r_s (p-value)	r_s (p-value)	r_s (p-value)	r_s (p-value)
Third order RMS	-0.047 (0.769)	-0.289 (0.064)	-0.076 (0.631)	-0.143 (0.366)
Fourth order RMS	0.048 (0.765)	-0.032 (0.840)	-0.035 (0.825)	0.068 (0.671)
Fifth order RMS	0.035 (0.825)	0.054 (0.736)	-0.049 (0.756)	0.068 (0.670)
Sixth order RMS	0.059 (0.710)	0.081 (0.611)	0.023 (0.886)	0.022 (0.889)
HOA RMS	-0.041 (0.795)	-0.288 (0.065)	-0.106 (0.506)	-0.143 (0.366)
Spherical aberration RMS	0.041 (0.795)	-0.111 (0.486)	-0.005 (0.975)	0.029 (0.853)
Coma aberration RMS	0.003 (0.984)	-0.054 (0.736)	0.003 (0.983)	-0.025 (0.873)
Z(3,-3)	0.087 (0.584)	0.239 (0.127)	0.108 (0.495)	0.159 (0.315)
Z(3,-1)	-0.199 (0.207)	-0.287 (0.065)	-0.272 (0.081)	-0.221 (0.160)
Z(3,1)	-0.266 (0.088)	-0.158 (0.319)	-0.177 (0.263)	-0.147 (0.353)
Z(3,3)	0.110 (0.489)	-0.032 (0.839)	0.106 (0.505)	-0.042 (0.790)
Z(4,-4)	-0.130 (0.411)	-0.197 (0.211)	-0.168 (0.289)	-0.058 (0.714)
Z(4,-2)	-0.240 (0.127)	-0.205 (0.194)	**-0.339* (0.028)**	-0.277 (0.076)
Z(4,0)	0.188 (0.233)	0.149 (0.346)	0.118 (0.456)	0.119 (0.453)
Z(4,2)	-0.291 (0.062)	-0.260 (0.096)	-0.153 (0.334)	-0.265 (0.090)
Z(4,4)	0.250 (0.110)	0.173 (0.273)	0.268 (0.086)	**0.342* (0.027)**
Z(5,-5)	-0.110 (0.487)	-0.168 (0.287)	-0.243 (0.122)	-0.050 (0.755)
Z(5,-3)	0.188 (0.232)	0.207 (0.189)	0.266 (0.089)	0.118 (0.457)
Z(5,-1)	0.201 (0.202)	0.242 (0.123)	0.116 (0.466)	0.123 (0.438)
Z(5,1)	-0.104 (0.512)	-0.088 (0.581)	-0.160 (0.310)	-0.194 (0.217)
Z(5,3)	0.076 (0.633)	0.146 (0.355)	0.037 (0.816)	0.109 (0.491)
Z(5,5)	-0.027 (0.867)	0.086 (0.586)	-0.129 (0.416)	0.008 (0.958)
Z(6,-6)	0.215 (0.172)	0.170 (0.280)	0.254 (0.105)	0.264 (0.092)
Z(6,-4)	0.176 (0.266)	0.100 (0.530)	**0.306* (0.049)**	0.034 (0.829)
Z(6,-2)	0.157 (0.321)	0.206 (0.190)	0.213 (0.176)	0.230 (0.142)
Z(6,0)	-0.165 (0.296)	-0.094 (0.552)	-0.166 (0.293)	-0.204 (0.195)
Z(6,2)	0.221 (0.159)	0.290 (0.062)	0.300 (0.053)	0.277 (0.076)
Z(6,4)	-0.260 (0.097)	-0.172 (0.275)	**-0.314* (0.043)**	**-0.323* (0.037)**
Z(6,6)	0.078 (0.624)	0.158 (0.317)	0.195 (0.216)	0.178 (0.259)

Table A3.5. Non-parametric correlations between the chromatic discrimination thresholds of the CAD test and corneal biomechanics parameters. IOPcc = corneal compensated intraocular pressure; IOPg = Goldmann correlated intraocular pressure; CRF = corneal resistance factor; CH = corneal hysteresis; r_s = Spearman's rank correlation coefficient. R = red; Y = yellow; G = green; B = blue.

	CAD	CAD R	CAD Y	CAD G	CAD B
	r_s (p-value)	r_s (p-value)	r_s (p-value)	r_s (p-value)	r_s (p-value)
IOPcc	0.076 (0.634)	0.162 (0.305)	-0.066 (0.678)	0.082 (0.604)	-0.029 (0.857)
IOPg	0.110 (0.489)	0.200 (0.203)	0.007 (0.965)	0.115 (0.468)	0.022 (0.889)
CRF	0.203 (0.197)	0.264 (0.091)	0.174 (0.270)	0.222 (0.158)	0.096 (0.547)
CH	0.167 (0.292)	0.197 (0.210)	0.172 (0.276)	0.182 (0.249)	0.110 (0.488)

Table A3.6. Non-parametric correlations between the chromatic discrimination thresholds of the CCT and the CCT quadrants with corneal biomechanics parameters and wavefront aberrations. IOPcc = corneal compensated intraocular pressure; IOPg = Goldmann correlated intraocular pressure; CRF = corneal resistance factor; CH = corneal hysteresis; r_s = Spearman's rank correlation coefficient. R = red; Y = yellow; G = green; B = blue; Q = quadrant.

	CCT	CCT Q1	CCT Q2	CCT Q3	CCT Q4
	r_s (p-value)	r_s (p-value)	r_s (p-value)	r_s (p-value)	r_s (p-value)
IOPcc	-0.180 (0.255)	-0.117 (0.462)	-0.253 (0.106)	-0.178 (0.261)	-0.104 (0.514)
IOPg	-0.127 (0.424)	-0.038 (0.812)	-0.213 (0.177)	-0.173 (0.274)	-0.031 (0.846)
CRF	0.060 (0.707)	0.138 (0.382)	-0.024 (0.878)	-0.010 (0.949)	0.097 (0.541)
CH	0.088 (0.579)	0.146 (0.355)	0.038 (0.813)	0.017 (0.915)	0.098 (0.538)

Table A3.7. Non-parametric correlations between the chromatic discrimination thresholds of the CCT hues and corneal biomechanics parameters and wavefront aberrations. IOPcc = corneal compensated intraocular pressure; IOPg = Goldmann correlated intraocular pressure; CRF = corneal resistance factor; CH = corneal hysteresis; r_s = Spearman's rank correlation coefficient. R = red; Y = yellow; G = green; B = blue.

	CCT R	CCT Y	CCT G	CCT B
	r_s (p-value)	r_s (p-value)	r_s (p-value)	r_s (p-value)
IOPcc	-0.144 (0.364)	-0.281 (0.071)	**-0.304* (0.050)**	-0.053 (0.740)
IOPg	-0.045 (0.778)	-0.243 (0.120)	-0.267 (0.087)	0.019 (0.905)
CRF	0.159 (0.314)	-0.087 (0.582)	0.002 (0.992)	0.122 (0.443)
CH	0.185 (0.242)	0.002 (0.990)	0.100 (0.530)	0.088 (0.581)

Table A3.8. Comparative analysis of chromatic discrimination thresholds of the CCT and of CCT quadrants for axial length and mean spherical equivalent between refractive error groups. AL = axial length; M = mean spherical equivalent; non = non-myopes; low = low myopes; moderate = moderate myopes; high = high myopes. SD = standard deviation; R = red; Y = yellow; G = green; B = blue.

Myopia degree		CCT		CCT Q1		CCT Q2		CCT Q3		CCT Q4	
		Mean± SD	H (p-value)	Mean± SD	H (p-value)	Mean± SD	H (p-value)	Mean± SD	H (p-value)	Mean± SD	H (p-value)
AL	small	0.0053±0.0011	1.175	0.0051±0.0012	0.681	0.0054±0.0009	0.982	0.0051±0.0013	2.729	0.0056±0.0012	0.535
	medium	0.0053±0.0010	(0.556)	0.0049±0.0010	(0.711)	0.0053±0.0010	(0.612)	0.0050±0.0010	(0.255)	0.0058±0.0013	(0.765)
	long	0.0053±0.0022		0.0050±0.0020		0.0055±0.0021		0.0049±0.0019		0.0059±0.0028	
M	non	0.0052±0.0011	1.542	0.0050±0.0012	0.917	0.0053±0.0010	1.480	0.0050±0.0012	2.467	0.0054±0.0012	1.295
	low	0.0055±0.0011	(0.673)	0.0051±0.0011	(0.821)	0.0055±0.0010	(0.687)	0.0052±0.0010	(0.481)	0.0061±0.0015	(0.730)
	moderate	0.0050±0.0007		0.0047±0.0008		0.0052±0.0009		0.0045±0.0006		0.0055±0.0009	
	high	0.0056±0.0028		0.0052±0.0025		0.0057±0.0027		0.0054±0.0025		0.0063±0.0035	

Table A3.9. Comparative analysis of chromatic discrimination thresholds of the CCT hues for axial length and mean spherical equivalent between refractive error groups. AL = axial length; M = mean spherical equivalent; non = non-myopes; low = low myopes; moderate = moderate myopes; high = high myopes. SD = standard deviation; R = red; Y = yellow; G = green; B = blue.

Myopia degree		CCT R		CCT Y		CCT G		CCT B	
		Mean± SD	H (p-value)	Mean± SD	H (p-value)	Mean± SD	H (p-value)	Mean± SD	H (p-value)
AL	small	0.0050±0.0011	0.959	0.0056±0.0010	0.937	0.0051±0.0014	2.805	0.0057±0.0013	0.662
	medium	0.0048±0.0011	(0.619)	0.0053±0.0010	(0.626)	0.0049±0.0010	(0.246)	0.0060±0.0014	(0.718)
	long	0.0049±0.0019		0.0056±0.0022		0.0047±0.0017		0.0061±0.0030	
M	non	0.0049±0.0011	1.398	0.0054±0.0011	1.474	0.0050±0.0013	2.240	0.0056±0.0012	1.244
	low	0.0051±0.0012	(0.706)	0.0055±0.0010	(0.688)	0.0051±0.0011	(0.524)	0.0063±0.0016	(0.743)
	moderate	0.0047±0.0008		0.0053±0.0009		0.0044±0.0006		0.0056±0.0010	
	high	0.0050±0.0024		0.0056±0.0028		0.0050±0.0021		0.0065±0.0037	

APPENDIX 4

The data presented in this Appendix illustrates the results obtained using the CAD and CCT colour vision tests for non-, low-, moderate- and high myopes.

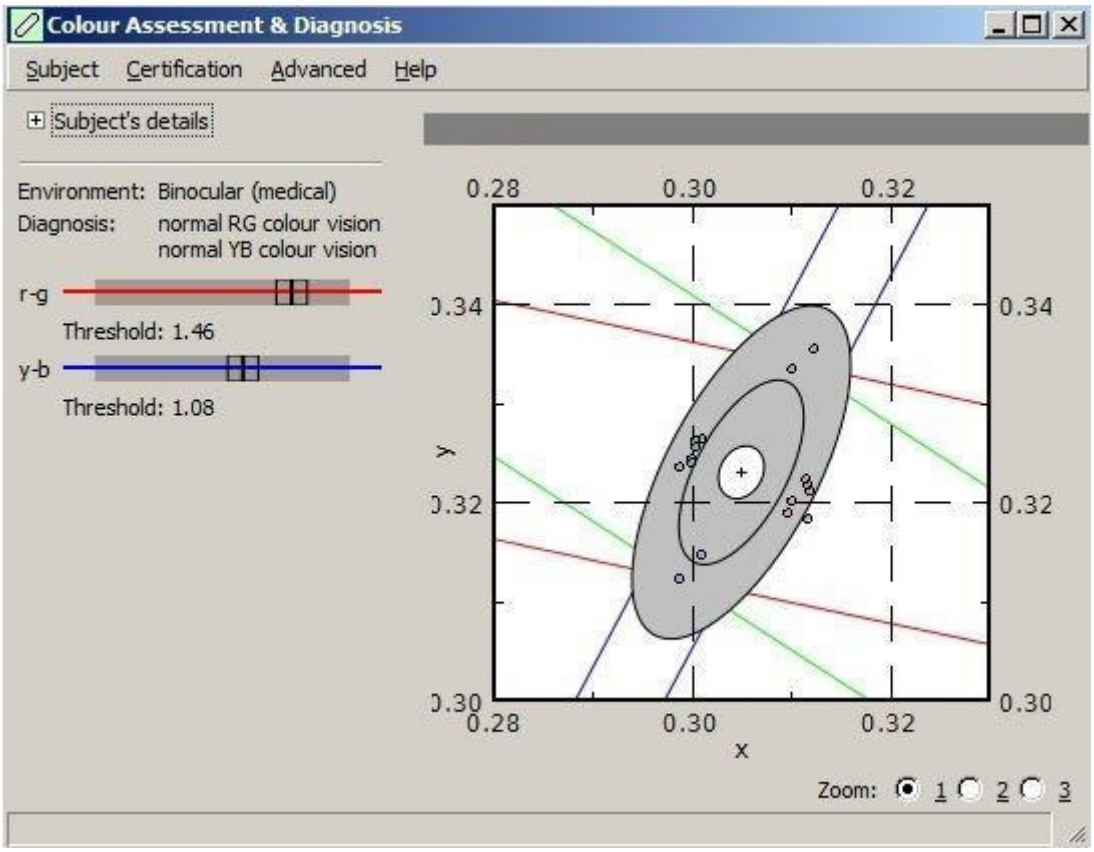

Figure A4. 1.Example of the CAD test results of a non-myopic subject.

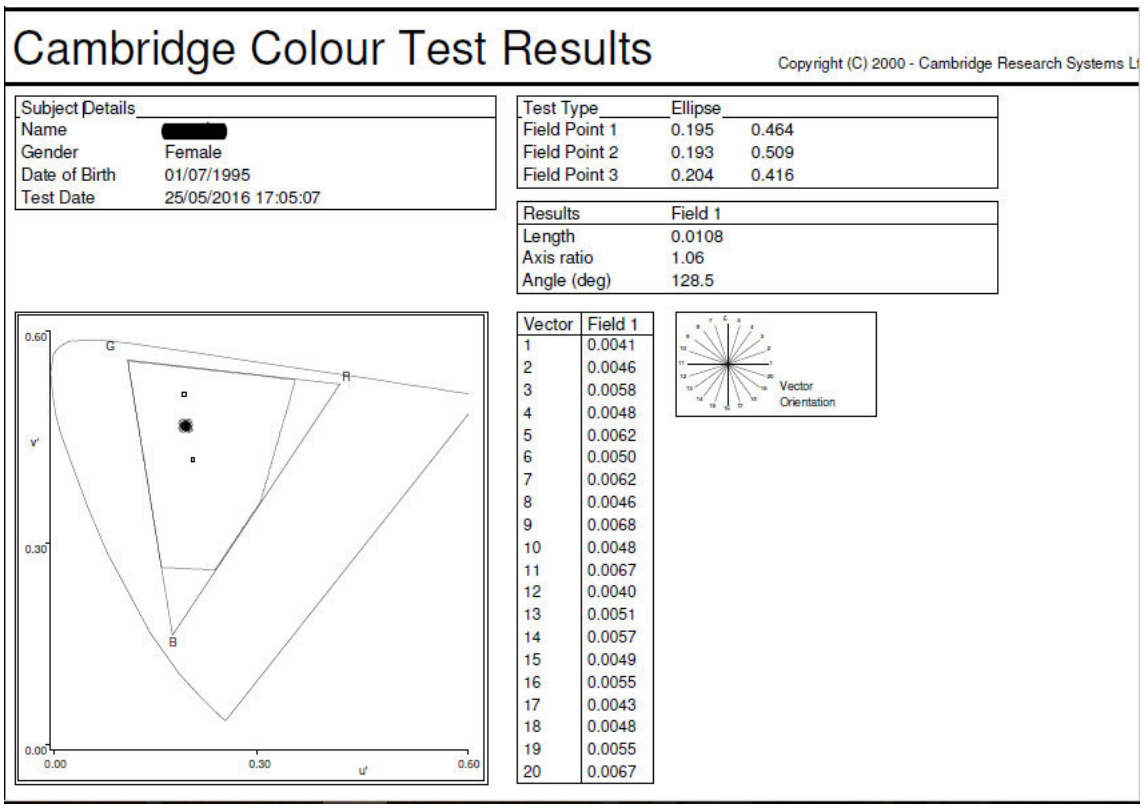

Figure A4. 2. Example of the CCT results of a non-myopic subject.

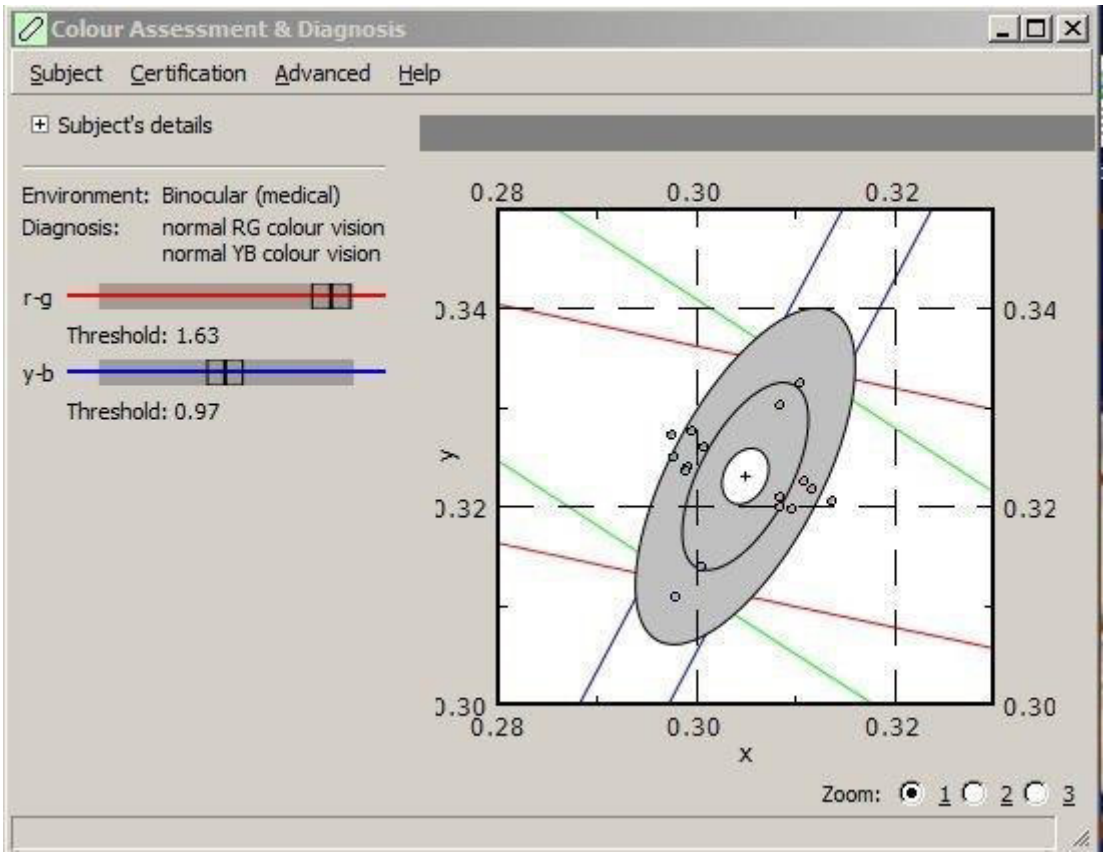

Figure A4. 3. Example of the CAD test results of a low-myopic subject.

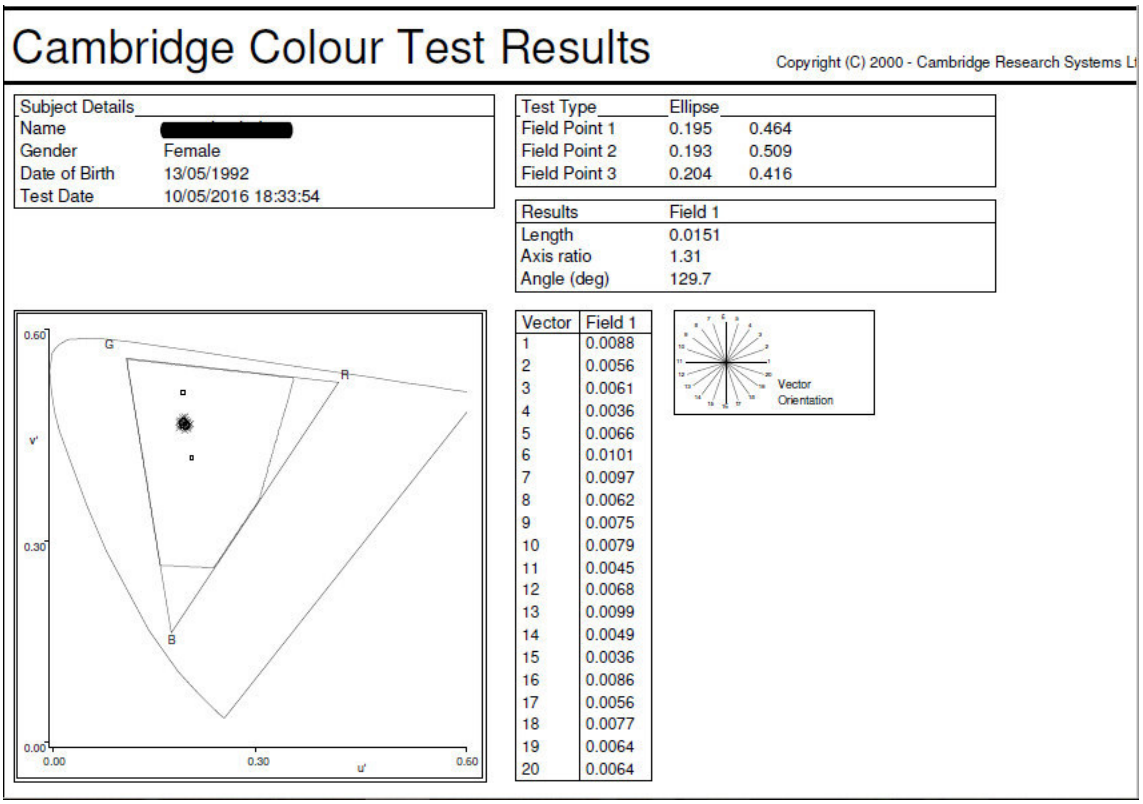

Figure A4. 4. Example of the CCT results of a low-myopic subject.

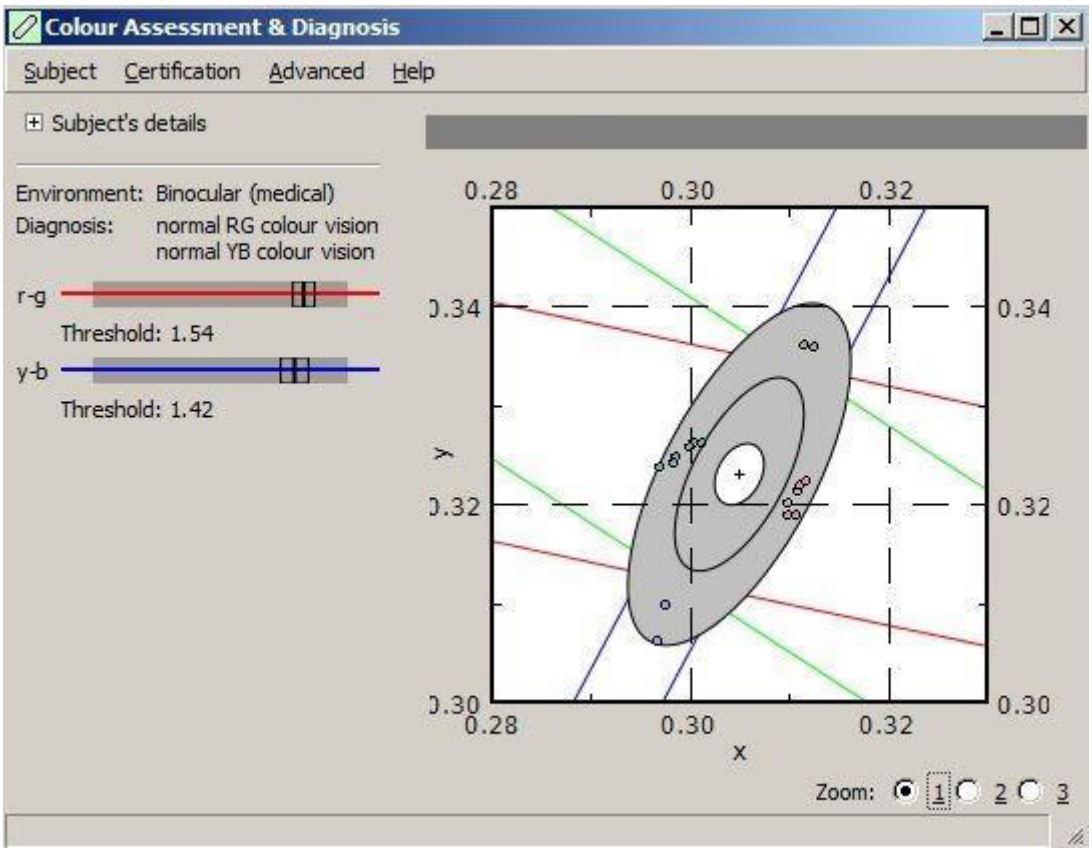

Figure A4. 5. Example of the CAD test results of a moderate-myopic subject.

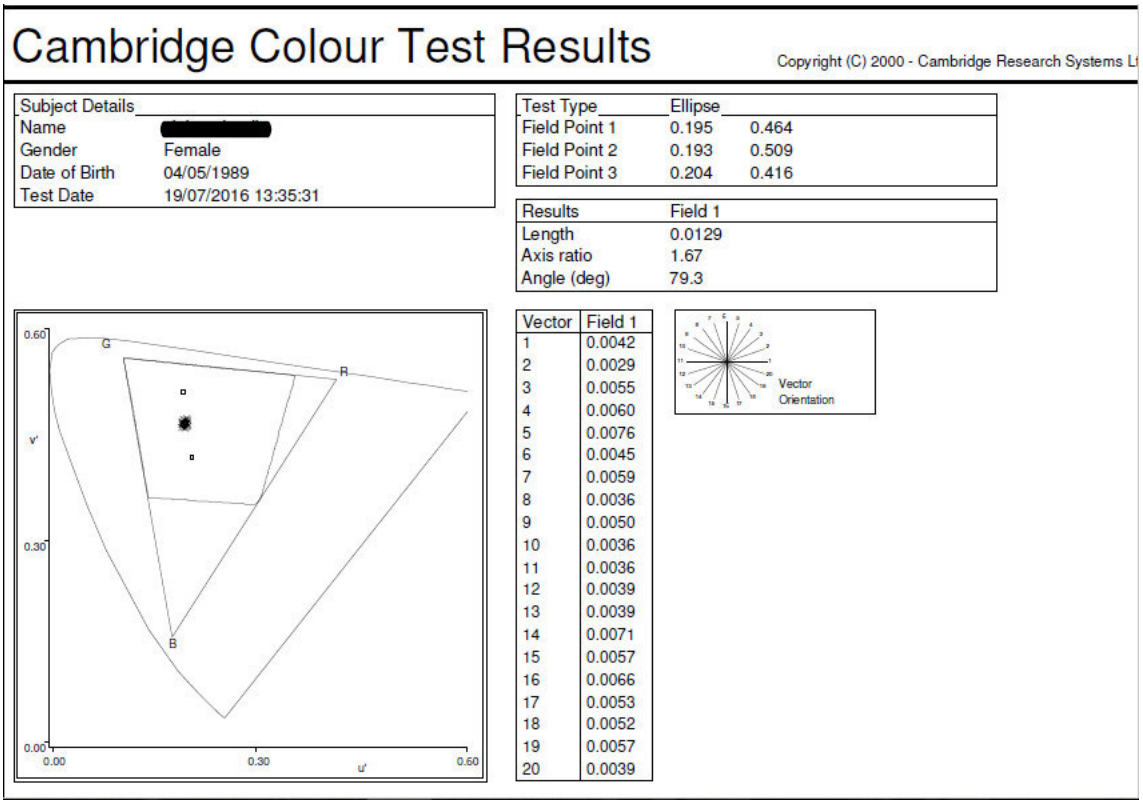

Figure A4. 6. Example of the CCT results of a moderate-myopic subject.

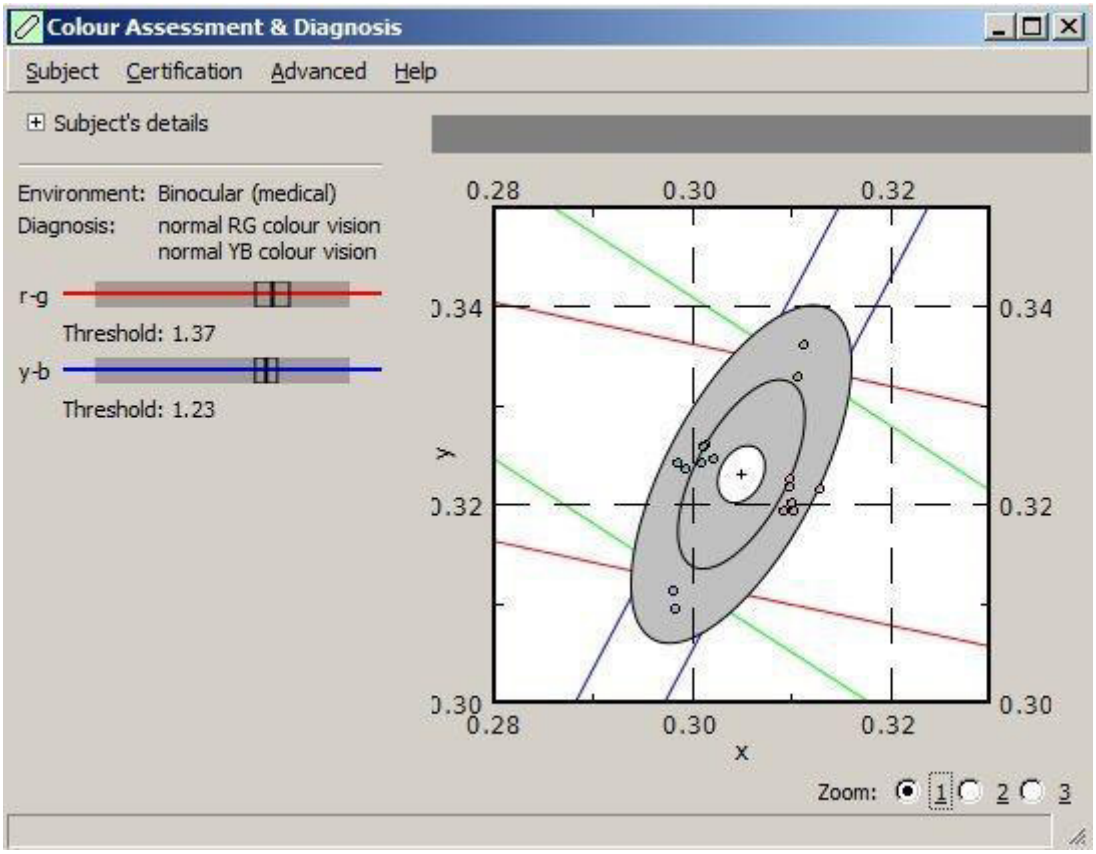

Figure A4. 7. Example of the CAD test results of a high-myopic subject.

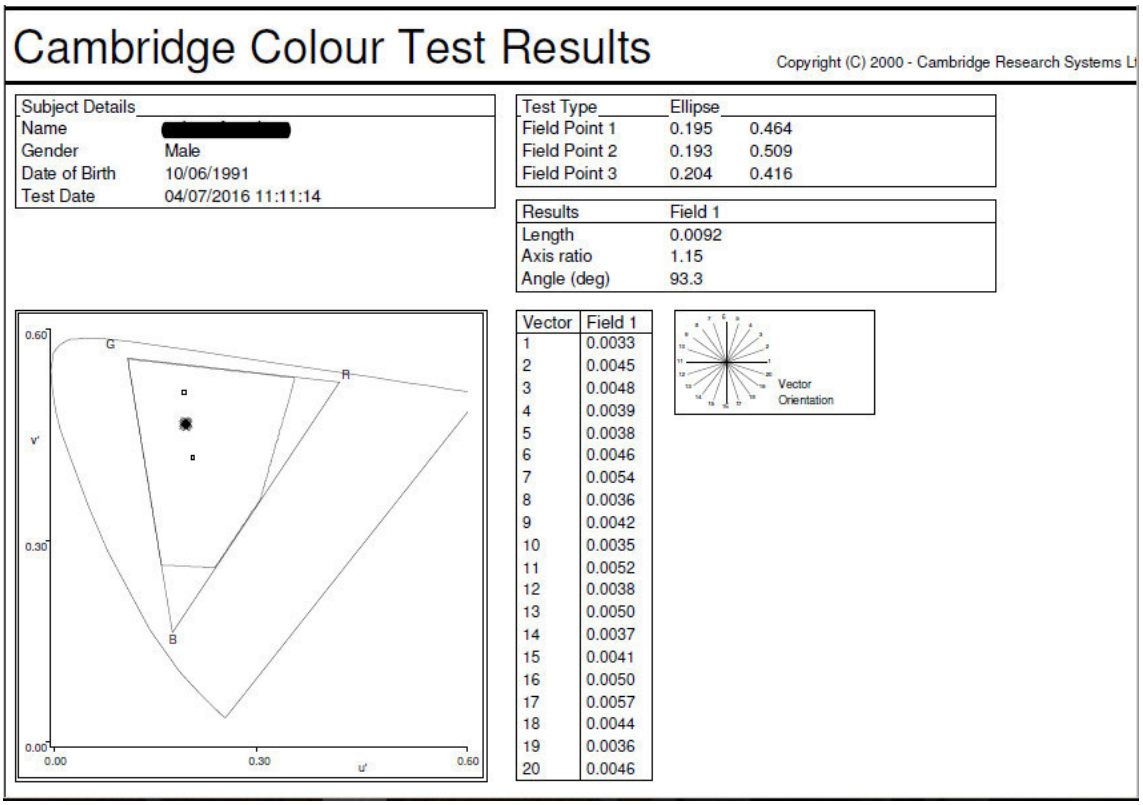

Figure A4. 8. Example of the CCT results of a high-myopic subject.